

The Emergence of Spatial Patterns for Compartmental Reaction Kinetics Coupled by Two Bulk Diffusing Species with Comparable Diffusivities

Merlin Pelz* and Michael J. Ward‡

Dept. of Mathematics, University of British Columbia, Vancouver, BC, Canada

January 18, 2023

Abstract

Originating from the pioneering study of Alan Turing, the bifurcation analysis predicting spatial pattern formation from a spatially uniform state for diffusing morphogens or chemical species that interact through nonlinear reactions is a central problem in many chemical and biological systems. From a mathematical viewpoint, one key challenge with this theory for two component systems is that stable spatial patterns can typically only occur from a spatially uniform state when a slowly diffusing “activator” species reacts with a much faster diffusing “inhibitor” species. However, from a modeling perspective, this large diffusivity ratio requirement for pattern formation is often unrealistic in biological settings since different molecules tend to diffuse with similar rates in extracellular spaces. As a result, one key long-standing question is how to robustly obtain pattern formation in the biologically realistic case where the time scales for diffusion of the interacting species are comparable. For a coupled 1-D bulk-compartment theoretical model, we investigate the emergence of spatial patterns for the scenario where two bulk diffusing species with comparable diffusivities are coupled to nonlinear reactions that occur only in localized “compartments”, such as on the boundaries of a 1-D domain. The exchange between the bulk medium and the spatially localized compartments is modeled by a Robin boundary condition with certain binding rates. As regulated by these binding rates, we show for various specific nonlinearities that our 1-D coupled PDE-ODE model admits symmetry-breaking bifurcations, leading to linearly stable asymmetric steady-state patterns, even when the bulk diffusing species have equal diffusivities. Depending on the form of the nonlinear kinetics, oscillatory instabilities can also be triggered. Moreover, the analysis is extended to treat a periodic chain of compartments.

Keywords Symmetry-breaking, localized compartments, pitchfork and Hopf bifurcations, reaction kinetics.

1 Introduction

In a pioneering study [48], Alan Turing showed that a spatially homogeneous steady-state solution of a reaction-diffusion (RD) system that is stable in the absence of diffusion can be destabilized in the presence of diffusing morphogens that have different diffusivities. From an application of this Turing stability theory to two-component activator-inhibitor systems, it is

*merlinpelz@math.ubc.ca

‡ward@math.ubc.ca (corresponding author)

Submitted to Proceedings of the Royal Society A.

well-known from a mathematical viewpoint that, for any activator-inhibitor reaction-kinetics admitting a stable fixed point, the ratio of the diffusivities of the inhibitor and activator species must be sufficiently large, i.e. above a threshold larger than unity, in order for spatially homogeneous patterns to emerge from the destabilization of a spatially uniform state (cf. [40], [1], [6]). Although this theoretically-predicted large diffusivity ratio requirement for pattern formation may be feasible to achieve in certain macroscale chemical systems, such as those involving a chemical species that can bind to a substrate (cf. [29], [8]), a large diffusivity ratio threshold in cellular biology is often unrealistic in applications where freely diffusing morphogen molecules have similar sizes and, consequently, comparable diffusivities. In scenarios where a large diffusivity ratio is a realistic assumption, two-component RD systems modeling chemical and biological systems typically admit a wide range of spatially localized patterns and instabilities that occur in the fully nonlinear regime (cf. [49], [50], [20], [21]).

From a theoretical viewpoint, there has been considerable focus on modifying the conventional two-component RD paradigm in order to circumvent the requirement of a large diffusivity ratio for the emergence of symmetry-breaking patterns. One such direction has involved extending the two-component RD system to include additional non-diffusible components (cf. [39], [24], [26]), which (roughly) models either membrane-bound proteins or other immobile chemically active substrates. This “2 + 1” extension can generate stable spatial patterns even when the diffusible species have a common diffusivity. In another direction, graph-theoretic properties such as network topology have been used for predicting Turing pattern formation for multi-component RD systems in the presence of immobile species (cf. [34], [7], [28]). More recently, it was shown in [19] using a probabilistic approach that as the number of species in a multi-component RD system increases, the required diffusivity ratio threshold for pattern formation is typically reduced.

A new direction for theoretical RD modeling, largely initiated in [14] and [30], involves exploring pattern-forming properties associated with coupling dynamically active spatially localized compartments via a bulk diffusion field. In a 1-D context, and with one bulk diffusing species, this modeling paradigm has been shown to lead to triggered oscillatory instabilities for various reaction kinetics (cf. [14], [16], [18], [15]), and whose bifurcation properties can be characterized via amplitude equations obtained from a weakly nonlinear analysis [37]. This 1-D such framework was used in [51] and [52] to model intracellular polarization and oscillations in fission yeast. Moreover, in multi-dimensional spatial geometries, pattern-forming properties of bulk-membrane RD systems have been studied both theoretically (cf. ([43], [9], [32], [31], [36])), and for certain specific biological applications, including cell polarization and Cdc42 protein pattern formation (cf. [4], [41], [42], [46], [38]).

The goal of this paper is to analyze symmetry-breaking pattern formation for a 1-D coupled bulk-compartment RD system in which spatially localized reaction compartments are coupled through a *two-component* linear bulk diffusion field with constant bulk degradation rates. The two-component reaction kinetics inside each compartment are assumed to be identical and the chemical exchange between the bulk medium and the spatially localized reaction compartments is modeled by a Robin boundary condition with certain binding rates. We refer to this modeling framework as a *compartmental-reaction diffusion system*. Although this coupled system does not admit spatially homogeneous steady-states, it does allow for the existence of steady-state solutions that are symmetric about the domain mid-line when the reaction compartments are identical. This symmetric steady-state solution is the *base state* for our analysis. From a linear stability analysis, and as confirmed by full PDE simulations, we will show for various specific activator-inhibitor intra-compartmental reaction kinetics that this coupled system admits symmetry-breaking pitchfork bifurcations of the symmetric base state, leading to *stable asymmetric steady-state patterns*, even when the bulk diffusing species have comparable or even *equal diffusivities*. We emphasize that the linear stability analysis predicting these symmetry-breaking bifurcations is more intricate than in [48] as it is based on a linearization around a *spatially non-uniform* symmetric steady-state, rather than around a spatially uniform steady-

state as in [48]. In our coupled system, a key parameter regulating the emergence of these stable asymmetric steady-states is shown to be a sufficiently large binding rate ratio of the two species on the compartment boundary. This feature is in contrast to the usual large diffusivity ratio requirement that is a necessary condition for pattern formation from a spatially uniform state for typical two-component activator-inhibitor RD systems (cf. [33], [27]).

A 2-D extension of the theoretical 1-D framework adopted in this article can potentially be applied to characterizing symmetry-breaking pattern-forming properties associated with biological or chemical modeling scenarios that involve small dynamically active, but spatially localized, discrete compartments or “cells” that are coupled through multi-component linear bulk diffusion fields. Examples of such problems include the original 2-D agent-based model of Rauch and Millonas [44] describing Turing pattern formation for cell-cell chemical signaling mediated by bulk diffusion, and the experimental study of [47] of Turing patterns associated with an emulsion of chemically loaded droplets dispersed in oil, in which the interdrop coupling is purely diffusive. The full agent-based numerical computations in [44] showed that nonlinear kinetic reactions restricted to lattice points on a 2-D lattice can generate stable Turing-type spatial patterns when coupled through a spatially discretized two-component bulk diffusion field where the diffusible species have a comparable diffusivity. The formulation of our theoretical model analyzed in a 1-D setting was inspired by this observation in [44].

The outline of this paper is as follows. In §2 we formulate and analyze a compartmental-reaction diffusion system when the reaction compartments are located on the boundaries of a 1-D spatial domain. For this model, symmetric and asymmetric steady-state solutions are determined for a class of reaction kinetics when the bulk diffusing species have comparable or equal diffusivities. This construction involves the solution of a nonlinear algebraic system, whose bifurcation structure can be used to predict pitchfork bifurcation points on the symmetric solution branch where asymmetric patterns emerge. Moreover, away from bifurcation points, the linear stability problem for the symmetric steady-state is studied numerically after first deriving a nonlinear matrix eigenvalue problem for the eigenvalue parameter. In this way, symmetry-breaking bifurcations of the symmetric steady-state, leading to stable asymmetric patterns, as the binding rate ratio increases past a threshold are illustrated for FitzHugh-Nagumo [14], Gierer-Meinhardt [12], and Rauch-Millonas [44] reaction kinetics. For FitzHugh-Nagumo kinetics we show that oscillatory instabilities of the symmetric steady-state are also possible in certain parameter regimes. In §3 we provide a similar analysis for a compartmental-reaction diffusion system where the localized reaction compartments are periodically spaced on a ring. For this periodic problem, symmetric steady-states are constructed analytically and, through a linear stability analysis based on a Floquet-type approach, we derive a nonlinear matrix eigenvalue problem that can be used to determine parameter values where symmetry-breaking bifurcations occur due to multiple possible modes of instability. The theory is illustrated for the three specific reaction kinetics. The theoretical predictions in §2 and §3 of symmetry-breaking bifurcations and stable asymmetric steady-states are confirmed from full time-dependent simulations of our PDE-ODE model. Owing to the novel form of the bulk-compartment coupling, off-the-shelf PDE software was not available for the PDE numerical simulations. The implicit-explicit (IMEX) numerical schemes and discretizations we developed for the full PDE simulations in §2 and §3 are derived in Appendix A and B, respectively.

2 Two Diffusion-Coupled Reaction Compartments

In our modeling framework, we assume that there is a compartment or “cell” located at each boundary of a one-dimensional spatial bulk domain $(0, L)$. These compartments are assumed to be reactive in the sense that two species with concentrations $\mu(t)$ and $\eta(t)$ are produced according to $\dot{\mu}(t) = f(\mu, \eta)$ and $\dot{\eta}(t) = g(\mu, \eta)$, for some nonlinear reaction kinetics f and g . Here the dot “ $\dot{\cdot}$ ” denotes the time derivative d/dt . Further, we assume that these two compartmental species are coupled to two bulk-defined species $u(t, x)$ and $v(t, x)$ on $(0, L)$ through a chemical exchange

across the compartment boundary. The bulk or extracellular species are assumed to undergo a linear diffusion process with constant diffusivities D_u and D_v and constant degradation rates σ_u and σ_v (see Fig. 1 for a schematic plot). This leads to a coupled PDE-ODE system formulated as

$$\text{bulk} \quad \begin{cases} \partial_t u = D_u \partial_{xx} u - \sigma_u u, & x \in (0, L) \\ \partial_t v = D_v \partial_{xx} v - \sigma_v v, & x \in (0, L) \end{cases} \quad (2.1a)$$

$$\text{reaction fluxes} \quad \begin{cases} D_u \partial_x u(t, 0) = \beta_u (u(t, 0) - \mu_1(t)) & \text{(Robin boundary conditions)} \\ D_v \partial_x v(t, 0) = \beta_v (v(t, 0) - \eta_1(t)) \\ -D_u \partial_x u(t, L) = \beta_u (u(t, L) - \mu_2(t)) \\ -D_v \partial_x v(t, L) = \beta_v (v(t, L) - \eta_2(t)) \end{cases} \quad (2.1b)$$

$$\text{compartments} \quad \begin{cases} \dot{\mu}_1 = f(\mu_1, \eta_1) + D_u \partial_x u(t, 0) & \text{(reaction kinetics at } x = 0) \\ \dot{\eta}_1 = g(\mu_1, \eta_1) + D_v \partial_x v(t, 0) \\ \dot{\mu}_2 = f(\mu_2, \eta_2) - D_u \partial_x u(t, L) & \text{(reaction kinetics at } x = L) \\ \dot{\eta}_2 = g(\mu_2, \eta_2) - D_v \partial_x v(t, L). \end{cases} \quad (2.1c)$$

To illustrate the analysis, in this section we will initially assume that the common reaction kinetics in the two compartments is the FitzHugh-Nagumo (FN) kinetics (with parameters $q > 0, z > 0, \varepsilon > 0$), as considered in [14], given by

$$f(\mu_j, \eta_j) = \mu_j - q(\mu_j - 2)^3 + 4 - \eta_j, \quad g(\mu_j, \eta_j) = \varepsilon \mu_j z - \varepsilon \eta_j, \quad (2.2)$$

for $j \in \{1, 2\}$. We refer to the parameters β_u and β_v in (2.1b) as the binding rates, as they model the strength of the exchange between the bulk and intra-compartmental species.

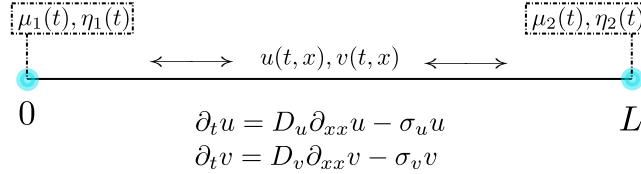


Figure 1: The domain $[0, L]$ with two diffusion-coupled compartments (cells) and intracellular reaction kinetics on its boundary.

2.1 Symmetry-breaking

With this formulation, we will calculate a steady-state solution that is symmetric in the sense that the concentrations in the two compartments are identical. By analyzing the linear stability of this steady-state, we will show that, depending on the parameters, it can be destabilized through either an oscillatory instability due to a Hopf bifurcation or from the emergence of a new stable steady-state that is asymmetric in the two compartments. In contrast to the typical Turing-type analysis for two component RD systems, this stable asymmetric steady-state for our model, which arises from a symmetry-breaking pitchfork bifurcation, occurs even when the bulk diffusivities are comparable.

2.1.1 Uncoupled system equilibrium

In the absence of diffusion, the ODE system for the intra-compartmental species is uncoupled from the bulk medium and reduces to

$$\dot{\mu}(t) = f(\mu, \eta), \quad \dot{\eta}(t) = g(\mu, \eta). \quad (2.3)$$

Let μ_e, η_e be an equilibrium point for (2.3) and label $F(\mu, \eta) := (f(\mu, \eta), g(\mu, \eta))$. For a specific parameter set, the linear stability property of the equilibrium state is characterized by whether the eigenvalues λ of the Jacobian $DF(\mu_e, \eta_e)$ have positive (unstable, exponentially growing perturbations) or negative (stable, exponentially decaying perturbations) real parts $\text{Re}(\lambda)$.

2.1.2 Coupled system equilibrium

In the presence of bulk diffusion, the compartments are coupled to the bulk medium. For this case, we first construct a steady-state solution for (2.1) without any symmetry assumptions.

In the bulk region $x \in (0, L)$, the steady-state solution for (2.1a) has the form

$$u_e(x) = A_1 \sinh(\omega_u(L-x)) + A_2 \sinh(\omega_u x), \quad v_e(x) = B_1 \sinh(\omega_v(L-x)) + B_2 \sinh(\omega_v x), \quad (2.4)$$

where $\omega_u := \sqrt{\sigma_u/D_u}$ and $\omega_v := \sqrt{\sigma_v/D_v}$. Here the constants A_1, A_2, B_1 and B_2 are to be determined. By employing the boundary conditions in (2.1b) for u , we obtain

$$\begin{pmatrix} A_1 \\ A_2 \end{pmatrix} = \frac{\beta_u}{D_u \omega_u (\gamma_u^2 - 1)} \begin{pmatrix} \gamma_u & 1 \\ 1 & \gamma_u \end{pmatrix} \begin{pmatrix} \mu_1^e \\ \mu_2^e \end{pmatrix} \quad \text{where} \quad \gamma_u := \cosh(\omega_u L) + \frac{\beta_u}{D_u \omega_u} \sinh(\omega_u L), \quad (2.5a)$$

while from the boundary conditions in (2.1b) for v we get

$$\begin{pmatrix} B_1 \\ B_2 \end{pmatrix} = \frac{\beta_v}{D_v \omega_v (\gamma_v^2 - 1)} \begin{pmatrix} \gamma_v & 1 \\ 1 & \gamma_v \end{pmatrix} \begin{pmatrix} \eta_1^e \\ \eta_2^e \end{pmatrix} \quad \text{where} \quad \gamma_v := \cosh(\omega_v L) + \frac{\beta_v}{D_v \omega_v} \sinh(\omega_v L). \quad (2.5b)$$

Next, from the compartmental reaction kinetics for the v -species in (2.1c), and from use of (2.4), we get

$$\frac{\beta_v}{\gamma_v^2 - 1} \tilde{A} \begin{pmatrix} \eta_1^e \\ \eta_2^e \end{pmatrix} = \begin{pmatrix} g(\mu_1^e, \eta_1^e) \\ g(\mu_2^e, \eta_2^e) \end{pmatrix} \quad \text{where} \quad \tilde{A} := \begin{pmatrix} \gamma_v \cosh(\omega_v L) - 1 & \cosh(\omega_v L) - \gamma_v \\ \cosh(\omega_v L) - \gamma_v & \gamma_v \cosh(\omega_v L) - 1 \end{pmatrix}. \quad (2.6)$$

For the special case where $g(\mu, \eta)$ is linear in η , i.e., $g(\mu, \eta) = g_1(\mu) - g_2 \eta$, as occurs for the FN kinetics in (2.2), we can use (2.6) to obtain

$$A \begin{pmatrix} \eta_1^e \\ \eta_2^e \end{pmatrix} = \begin{pmatrix} g_1(\mu_1^e) \\ g_1(\mu_2^e) \end{pmatrix} \quad \text{with} \quad A := \frac{\beta_v}{\gamma_v^2 - 1} \tilde{A} + g_2 I, \quad (2.7)$$

where I is the identity matrix.

Next, we use (2.4) in (2.1c) for the u -species. This yields

$$\frac{\beta_u}{\gamma_u^2 - 1} B \begin{pmatrix} \mu_1^e \\ \mu_2^e \end{pmatrix} = \begin{pmatrix} f(\mu_1^e, \eta_1^e) \\ f(\mu_2^e, \eta_2^e) \end{pmatrix} \quad \text{where} \quad B := \begin{pmatrix} \gamma_u \cosh(\omega_u L) - 1 & \cosh(\omega_u L) - \gamma_u \\ \cosh(\omega_u L) - \gamma_u & \gamma_u \cosh(\omega_u L) - 1 \end{pmatrix}. \quad (2.8)$$

Finally, by solving (2.7) for η_1^e and η_2^e , we substitute the resulting expressions into (2.8) to obtain a nonlinear algebraic system for μ_1^e and μ_2^e

$$\begin{pmatrix} f(\mu_1^e, (1, 0)(\frac{\beta_v}{\gamma_v^2 - 1} \tilde{A} + g_2 I)^{-1} (g_1(\mu_1^e), g_1(\mu_2^e))^T) \\ f(\mu_2^e, (0, 1)(\frac{\beta_v}{\gamma_v^2 - 1} \tilde{A} + g_2 I)^{-1} (g_1(\mu_1^e), g_1(\mu_2^e))^T) \end{pmatrix} - \frac{\beta_u}{\gamma_u^2 - 1} B \begin{pmatrix} \mu_1^e \\ \mu_2^e \end{pmatrix} = 0, \quad (2.9)$$

where T denotes transposition. In terms of a solution to (2.9) we can determine the other steady-state values from (2.8) and (2.5). We emphasize that (2.9) applies to all steady-states of (2.1) regardless of symmetry.

The matrices A and B that effectively couple the two compartments are symmetric and circulant, and hence have the common eigenspace spanned by $q_1 := (1, 1)^T$ and $q_2 := (1, -1)^T$. The corresponding eigenvalues a_j and b_j for A and B for $j = 1, 2$ are simply

$$\begin{aligned} Aq_1 &= \left(\frac{\beta_v}{\gamma_v^2 - 1} (\gamma_v (\cosh(\omega_v L) - 1) + (\cosh(\omega_v L) - 1)) + g_2 \right) q_1 = a_1 q_1, \\ Aq_2 &= \left(\frac{\beta_v}{\gamma_v^2 - 1} (\gamma_v (\cosh(\omega_v L) + 1) - (\cosh(\omega_v L) + 1)) + g_2 \right) q_2 = a_2 q_2, \\ Bq_1 &= (\gamma_u (\cosh(\omega_u L) - 1) + (\cosh(\omega_u L) - 1)) q_1 = b_1 q_1, \\ Bq_2 &= (\gamma_u (\cosh(\omega_u L) + 1) - (\cosh(\omega_u L) + 1)) q_2 = b_2 q_2. \end{aligned} \quad (2.10)$$

To determine a symmetric solution for (2.9) for which $(\mu_1^e, \mu_2^e) = \mu_e q_1$, where $q_1 = (1, 1)^T$, we simply use the eigenvalues a_1 and b_1 in (2.10) to reduce (2.9) to

$$f\left(\mu_e, \frac{g_1(\mu_e)}{a_1}\right) - \frac{\beta_u}{\gamma_u^2 - 1} b_1 \mu_e = 0. \quad (2.11)$$

This scalar nonlinear algebraic problem for μ_e applies whenever $g(\mu, \eta)$ has the specific form $g(\mu, \eta) = g_1(\mu) - g_2 \eta$, where g_2 is a constant.

To detect any symmetry-breaking pitchfork bifurcation points of the symmetric steady-state solution we can perform a linear stability analysis of (2.1) around the steady-state solution and seek $\lambda = 0$ eigenvalue crossings. More conveniently, to detect zero-eigenvalue crossings for the linearization of the full system (2.1) we can more simply determine bifurcation points associated with the linearization of the nonlinear algebraic system (2.9) around a symmetric steady-state. To do so, we introduce the perturbation $(\mu_1, \mu_2)^T = \mu_e q_1 + \delta \phi$ from the symmetric steady-state into (2.9) to obtain, for $\delta \ll 1$, the linearized problem

$$\begin{pmatrix} \frac{d}{d\mu_1} f(\mu_1, (1, 0)A^{-1}(g_1(\mu_1), g_1(\mu_2))^T) & \frac{d}{d\mu_2} f(\mu_1, (1, 0)A^{-1}(g_1(\mu_1), g_1(\mu_2))^T) \\ \frac{d}{d\mu_1} f(\mu_2, (0, 1)A^{-1}(g_1(\mu_1), g_1(\mu_2))^T) & \frac{d}{d\mu_2} f(\mu_2, (0, 1)A^{-1}(g_1(\mu_1), g_1(\mu_2))^T) \end{pmatrix} \phi - \frac{\beta_u}{\gamma_u^2 - 1} B \phi = 0, \quad (2.12)$$

where the derivatives are to be evaluated at the symmetric state $\mu_1 = \mu_e$ and $\mu_2 = \mu_e$. In this way, we obtain the linearized problem

$$\begin{pmatrix} J_{11} & J_{12} \\ J_{21} & J_{22} \end{pmatrix} \phi - \frac{\beta_u}{\gamma_u^2 - 1} B \phi = 0, \quad (2.13a)$$

where the Jacobian matrix coefficients are given, in terms of any solution μ_e of (2.11), by

$$J_{11} := \partial_{\mu} f\left(\mu_e, \frac{g_1(\mu_e)}{a_1}\right) + \partial_{\eta} f\left(\mu_e, \frac{g_1(\mu_e)}{a_1}\right) (1, 0) A^{-1} (g_1'(\mu_e), 0)^T, \quad (2.13b)$$

$$J_{12} := \partial_{\eta} f\left(\mu_e, \frac{g_1(\mu_e)}{a_1}\right) (1, 0) A^{-1} (0, g_1'(\mu_e))^T, \quad (2.13c)$$

$$J_{21} := \partial_{\eta} f\left(\mu_e, \frac{g_1(\mu_e)}{a_1}\right) (0, 1) A^{-1} (g_1'(\mu_e), 0)^T, \quad (2.13d)$$

$$J_{22} := \partial_{\mu} f\left(\mu_e, \frac{g_1(\mu_e)}{a_1}\right) + \partial_{\eta} f\left(\mu_e, \frac{g_1(\mu_e)}{a_1}\right) (0, 1) A^{-1} (0, g_1'(\mu_e))^T. \quad (2.13e)$$

From (2.13), a bifurcation with an in-phase perturbation $\phi = q_1$, if it exists, must satisfy

$$\partial_{\mu} f\left(\mu_e, \frac{g_1(\mu_e)}{a_1}\right) + \partial_{\eta} f\left(\mu_e, \frac{g_1(\mu_e)}{a_1}\right) \frac{g_1'(\mu_e)}{a_1} - \frac{\beta_u}{\gamma_u^2 - 1} b_1 = 0. \quad (2.14)$$

Moreover, a bifurcation with an anti-phase perturbation $\phi = q_2$, if it exists, has to fulfill

$$\partial_{\mu} f\left(\mu_e, \frac{g_1(\mu_e)}{a_1}\right) + \partial_{\eta} f\left(\mu_e, \frac{g_1(\mu_e)}{a_1}\right) \frac{g_1'(\mu_e)}{a_2} - \frac{\beta_u}{\gamma_u^2 - 1} b_2 = 0. \quad (2.15)$$

Below in §2.2.1 we will show for FN kinetics that the symmetric steady-state is never destabilized through a zero-eigenvalue crossing of the linearization with an in-phase perturbation. In contrast, to find a bifurcation point for an anti-phase eigenperturbation, we must solve the following coupled system for μ_e and a bifurcation parameter:

$$f\left(\mu_e, \frac{g_1(\mu_e)}{a_1}\right) - \frac{\beta_u}{\gamma_u^2 - 1} b_1 \mu_e = 0, \quad (2.16a)$$

$$\partial_{\mu} f\left(\mu_e, \frac{g_1(\mu_e)}{a_1}\right) + \partial_{\eta} f\left(\mu_e, \frac{g_1(\mu_e)}{a_1}\right) \frac{g_1'(\mu_e)}{a_2} - \frac{\beta_u}{\gamma_u^2 - 1} b_2 = 0. \quad (2.16b)$$

The bifurcation parameter is taken either as a reaction kinetic parameter or as the ratio $\rho := \beta_v/\beta_u$ of the binding rates. In (2.16) the explicit expressions for the matrix eigenvalues a_1 , a_2 , b_1 , and b_2 are defined in (2.10) in terms of the parameters.

2.2 Compartments with FitzHugh-Nagumo kinetics

2.2.1 Application of the theory

When uncoupled from the bulk, the intra-compartmental dynamics with FN kinetics is (see [14])

$$\dot{\mu} = f(\mu, \eta) := \mu - q(\mu - 2)^3 + 4 - \eta, \quad \dot{\eta} = g(\mu, \eta) := \varepsilon z \mu - \varepsilon \eta. \quad (2.17)$$

As shown in §2 of [18], there are up to three equilibria for (2.17) that are determined by the cubic

$$\mu_e - q(\mu_e - 2)^3 + 4 - z\mu_e = 0.$$

With $F(\mu, \eta) := (f(\mu, \eta), g(\mu, \eta))$, and for a specific parameter set, the sign of the real parts of the eigenvalues of $DF(\mu_e, \eta_e)$ can be read off the tr-det-plot with, in this setting, $\text{tr}(DF(\mu_e, \eta_e)) = 1 - 3q(\mu_e - 2)^2 - \varepsilon$ and $\det(DF(\mu_e, \eta_e)) = 3\varepsilon q(\mu_e - 2)^2 + \varepsilon(z - 1)$. For $z > 1$, for which $\det(DF(\mu_e, \eta_e)) > 0$, the linear stability of μ_e is determined by the sign of $\text{tr}(DF(\mu_e, \eta_e))$. We will choose a parameter set for which there is a unique linearly stable steady-state of the intra-compartmental dynamics (2.17) (see the green dot in Fig. 2).

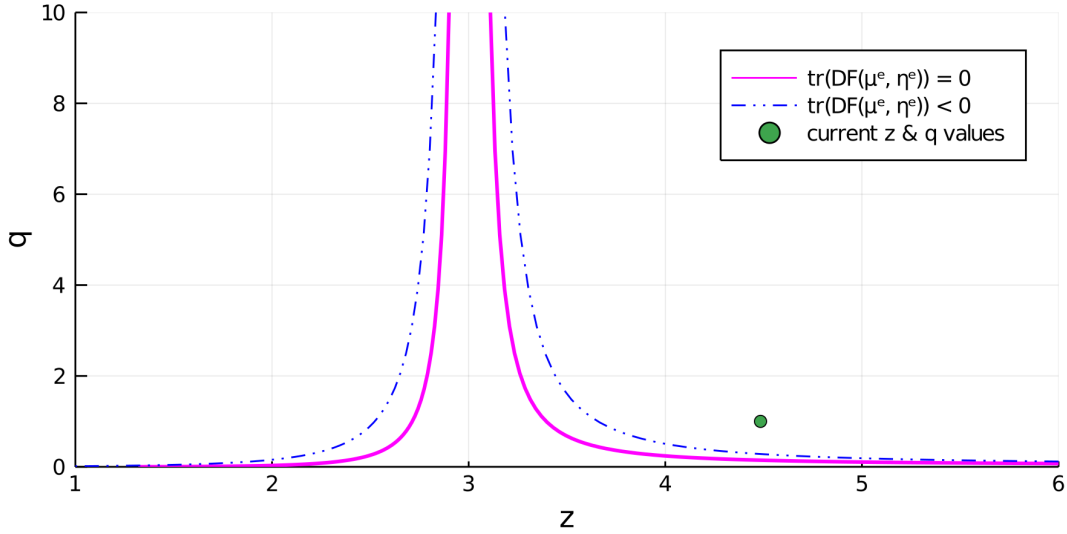


Figure 2: The instability boundary $\text{tr}(DF(\mu_e, \eta_e)) = 0$ (magenta curve) in the (q, z) -plane for a unique steady-state of (2.17) with $\varepsilon = 0.7$, and a generic curve (blue curve) where the steady-state is linearly stable. For $q = 1$ and $z = 4.48430$ (green dot) there is a unique stable steady state $\mu_e \approx 1.26293$ and $\eta_e = z\mu_e \approx 5.66336$ for which $\text{tr}(DF(\mu_e, \eta_e)) \approx -1.32981 < 0$.

To apply the steady-state theory of §2.1.2 for the bulk-cell coupled system for FN kinetics we first identify that $g(\mu, \eta) = g_1(\mu) - g_2\eta$, where $g_1 = \varepsilon\mu z$ and $g_2 = \varepsilon$. From (2.7) we get

$$A \begin{pmatrix} \eta_1^e \\ \eta_2^e \end{pmatrix} = \varepsilon z \begin{pmatrix} \mu_1^e \\ \mu_2^e \end{pmatrix} \quad \text{with} \quad A := \frac{\beta_v}{\gamma_v^2 - 1} \tilde{A} + \varepsilon I, \quad (2.18)$$

where \tilde{A} was defined in (2.6). In terms of A , we obtain from (2.9) that the nonlinear algebraic system characterizing both symmetric and asymmetric steady-states is

$$\begin{pmatrix} \mu_1^e \\ \mu_2^e \end{pmatrix} - q \begin{pmatrix} (\mu_1^e - 2)^3 \\ (\mu_2^e - 2)^3 \end{pmatrix} + 4 \begin{pmatrix} 1 \\ 1 \end{pmatrix} - \varepsilon z A^{-1} \begin{pmatrix} \mu_1^e \\ \mu_2^e \end{pmatrix} - \frac{\beta_u}{\gamma_u^2 - 1} B \begin{pmatrix} \mu_1^e \\ \mu_2^e \end{pmatrix} = 0. \quad (2.19)$$

From (2.11), the symmetric steady-state solution, for which $\mu_1^e = \mu_2^e = \mu_e$, is obtained from

$$-q(\mu_e - 2)^3 + 4 + \left(1 - \frac{\varepsilon z}{a_1} - \frac{\beta_u}{\gamma_u^2 - 1} b_1\right) \mu_e = 0, \quad (2.20)$$

where a_1 is an eigenvalue of A as defined in (2.10) with $g_2 = \varepsilon$.

Bifurcation points (if they exist) for either in-phase and anti-phase perturbations of the symmetric steady-state, as obtained from (2.16), satisfy

$$-3q(\mu_e - 2)^2 + 1 - \frac{\varepsilon z}{a_1} - \frac{\beta_u}{\gamma_u^2 - 1} b_1 = 0, \quad (\text{in-phase}) \quad (2.21a)$$

$$-3q(\mu_e - 2)^2 + 1 - \frac{\varepsilon z}{a_2} - \frac{\beta_u}{\gamma_u^2 - 1} b_2 = 0, \quad (\text{anti-phase}) \quad (2.21b)$$

where a_1, a_2, b_1, b_2 are the eigenvalues of A and B as given in (2.10) with $g_2 = \varepsilon$.

To show that there can be no bifurcation point for the in-phase perturbation of the symmetric steady-state when $\mu_e \geq -1$, we use (2.21a) in (2.20) to eliminate $\varepsilon z/a_1 + \beta_u/(\gamma_u^2 - 1)$. This yields

$$\begin{aligned} 0 &= q(\mu_e - 2)^3 - 4 + \left(\frac{\varepsilon z}{a_1} + \frac{\beta_u}{\gamma_u^2 - 1} b_1 - 1 \right) \mu_e \\ &= q(\mu_e - 2)^2((\mu_e - 2) - 3\mu_e) - 4 = -2q(\mu_e - 2)^2(\mu_e + 1) - 4 \leq 0, \end{aligned}$$

which shows that a bifurcation with an in-phase eigenperturbation is impossible when $\mu_e \geq -1$.

To determine a bifurcation point associated with the anti-phase perturbation of the symmetric steady-state we must solve the coupled system (2.21b) and (2.20) on the range where $\varepsilon z/a_2 + \beta_u b_2/(\gamma_u^2 - 1) \leq 1$. By eliminating μ_e between (2.21b) and (2.20) we obtain

$$q - \frac{\left(1 - \frac{\varepsilon z}{a_2} - \frac{\beta_u}{\gamma_u^2 - 1} b_2\right)}{27 \left(6 - \frac{2\varepsilon z}{a_1} - \frac{2\beta_u}{\gamma_u^2 - 1} b_1\right)^2} \left(-2 + \varepsilon z \left(\frac{3}{a_1} - \frac{1}{a_2}\right) + \frac{\beta_u}{\gamma_u^2 - 1} (3b_1 - b_2)\right)^2 = 0. \quad (2.22)$$

For a fixed parameter set, we view the parameter constraint (2.22) as a nonlinear algebraic equation for either z or for the binding rate ratio $\rho := \beta_v/\beta_u$.

In terms of z , in Fig. 3(left) we plot both symmetric and asymmetric steady-state solution branches, as computed from (2.20) and (2.19) using MatCont [5] for the parameter set given in the figure caption. We observe that asymmetric steady-state solution branches form a bubble structure between two pitchfork bifurcation points $z_{P,1}$ and $z_{P,2}$ associated with anti-phase perturbations of the symmetric steady-state. For $z = z_{P,1}$, in Fig. 3(right) we plot symmetric and asymmetric solution branches in terms of $\rho := \beta_v/\beta_u$ for the same parameter set in Fig. 3(left). This latter figure shows the existence of a symmetry-breaking bifurcation as the binding rate ratio ρ increases past a critical value, and where the bulk diffusivity ratio is fixed near unity.

2.2.2 Hopf bifurcation bubble

The analysis in (2.2.1) has constructed both symmetric and asymmetric equilibria of the coupled bulk-cell model with FN kinetics and has detected symmetry-breaking bifurcations of the symmetric solution branch u_e, v_e, μ_e, η_e that correspond to zero-eigenvalue crossings of the linear stability problem.

We now formulate and study the linear stability problem for the symmetric steady-state solution branch to determine whether other instabilities, such as Hopf bifurcations, are possible. For the linear stability analysis we perturb the symmetric steady-state by introducing $u(t, x) = u_e(x) + \phi(x)e^{\lambda t}$, $v(t, x) = v_e(x) + \psi(x)e^{\lambda t}$, $\mu_j(t) = \mu_e + \xi_j e^{\lambda t}$, $\eta = \eta_e + \zeta_j e^{\lambda t}$, where $|\phi| \ll 1$, $|\psi| \ll 1$, $|\xi_j| \ll 1$ and $|\zeta_j| \ll 1$ for $j \in \{1, 2\}$, into (2.1) and linearizing. This yields the linearized

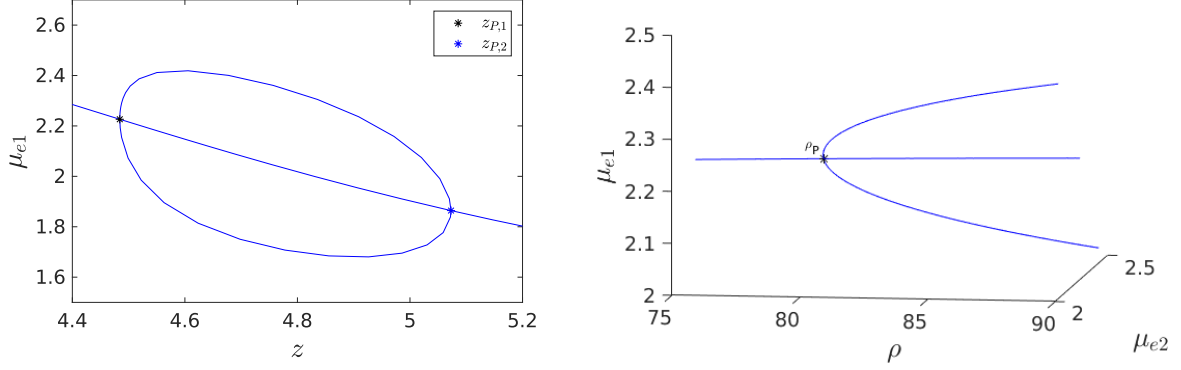


Figure 3: Left: μ_{e1}^e versus z showing that asymmetric equilibria exist inside a pitchfork bubble delimited by $z_{P,1} \approx 4.48430$ and $z_{P,2} \approx 5.07294$ when $\rho = \beta_v/\beta_u = 80$. Right: For $z = z_{P,1}$, there is a symmetry-breaking bifurcation of the symmetric steady-state as ρ increases past the critical value $\rho_p = 80$. Parameters: $D_u = 1, D_v = 3, \sigma_u = \sigma_v = 1, \varepsilon = 0.7, q = 1, L = 1$, and $\beta_u = 0.1$.

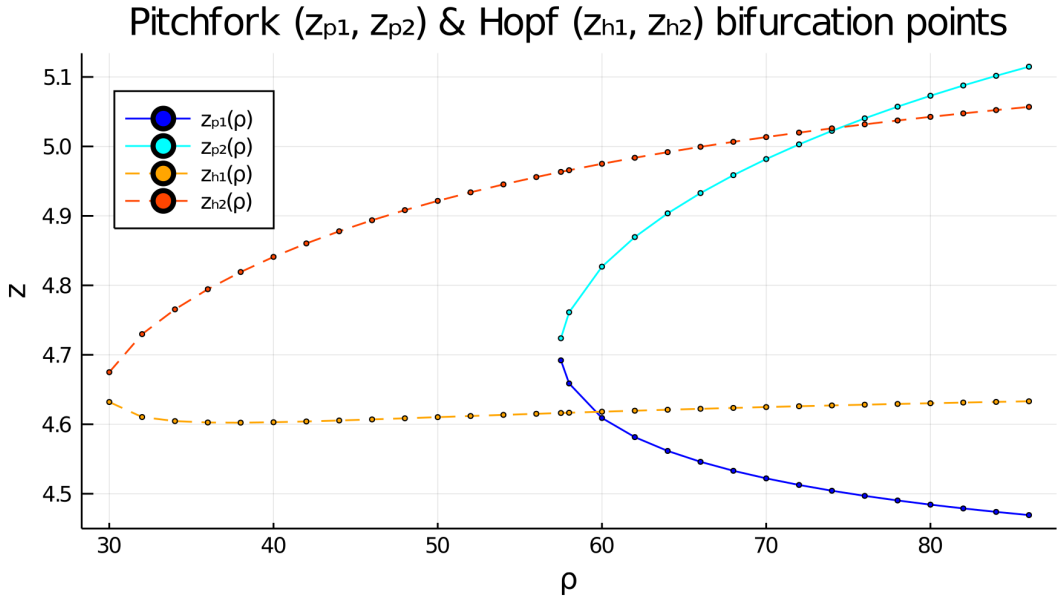


Figure 4: Symmetry-breaking pitchfork bifurcation thresholds $z_{P,1}$ and $z_{P,2}$ versus ρ corresponding to zero-eigenvalue crossings for the anti-phase mode where the asymmetric steady-state bifurcates from the symmetric branch. The anti-phase mode is unstable on the range $z_{P,1} < z < z_{P,2}$. The symmetric branch is unstable to an oscillatory instability for the in-phase mode when $z_{H,1} < z < z_{H,2}$, where $z_{H,1}$ and $z_{H,2}$ are Hopf bifurcation thresholds for the in-phase mode. On the range $\rho > 75$, we observe the ordering $z_{P,1} < z_{H,1} < z_{H,2} < z_{P,2}$. For this range of ρ , where the unstable oscillatory range for the in-phase mode is contained within the pitchfork range, the asymmetric branches of equilibria that bifurcate from the symmetric branch are predicted to be locally linearly stable. Parameters: $D_u = 1, D_v = 3, \sigma_u = \sigma_v = 1, \varepsilon = 0.7, q = 1, L = 1$, $\beta_u = 0.1$, and $\beta_v = \rho\beta_u$.

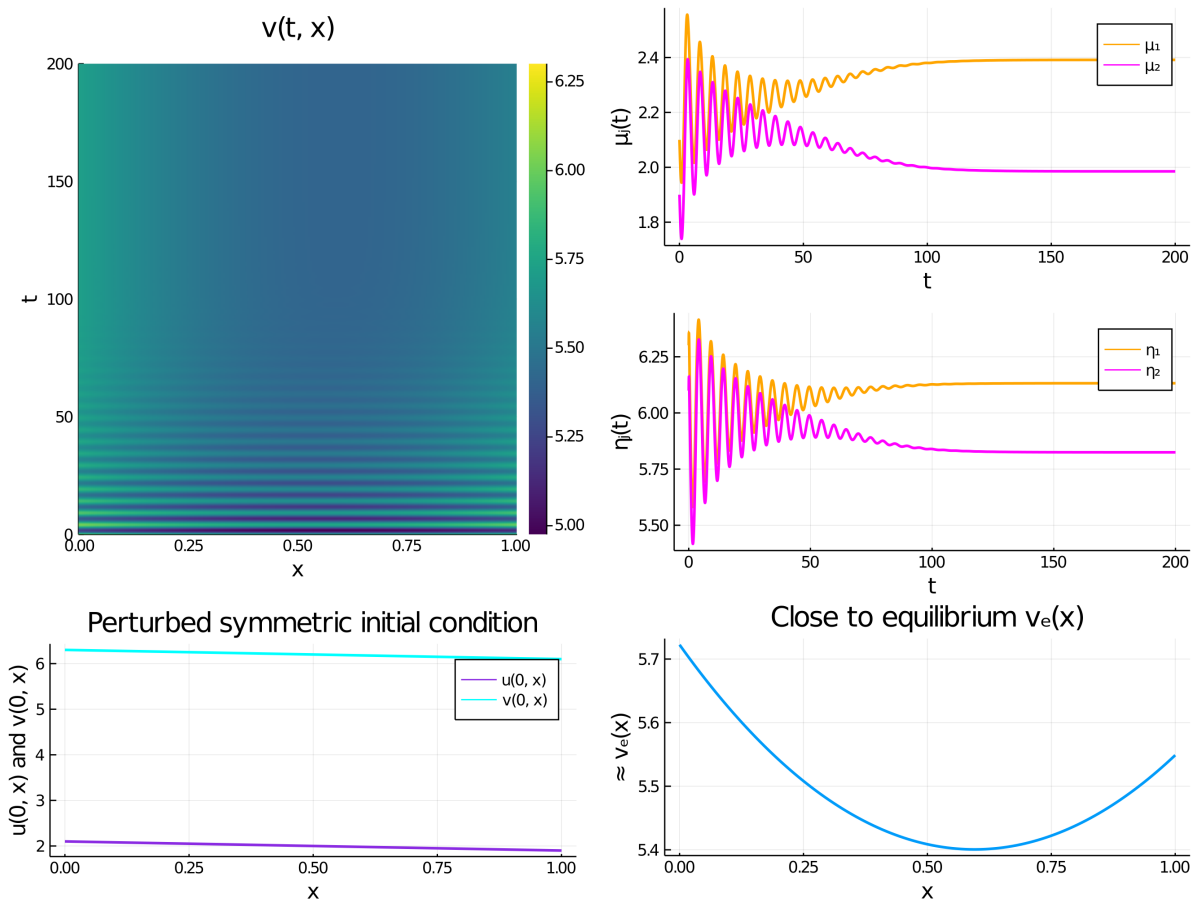


Figure 5: For an initial condition near the unstable symmetric branch, and for $z = 4.52211$ and $\rho = 80$, we predict that the asymmetric solution branch is linearly stable since $z_{P,1} < z < z_{H,1}$ (see Fig. 4). The full PDE simulation of (2.1) by the CN-RK4 IMEX method of Appendix A supports this conjecture and shows the existence of a stable asymmetric steady-state. For $z = 4.52211$, the ρ -pitchfork point was $\rho \approx 70$ (see Fig. 4). Parameters: $D_u = 1, D_v = 3, \sigma_u = \sigma_v = 1, \varepsilon = 0.7, q = 1, L = 1, \beta_u = 0.1, \rho = \beta_v/\beta_u = 80$.

eigenvalue problem

$$\text{bulk} \quad \begin{cases} \partial_{xx}\phi - \Omega_u^2\phi = 0, & x \in (0, L) \\ \partial_{xx}\psi - \Omega_v^2\psi = 0, & x \in (0, L) \end{cases} \quad (2.23a)$$

$$\text{reaction fluxes} \quad \begin{cases} D_u\partial_x\phi(0) = \beta_u(\phi(0) - \xi_1) \\ D_v\partial_x\psi(0) = \beta_v(\psi(0) - \zeta_1) \\ -D_u\partial_x\phi(L) = \beta_u(\phi(L) - \xi_2) \\ -D_v\partial_x\psi(L) = \beta_v(\psi(L) - \zeta_2) \end{cases} \quad \begin{array}{l} \text{(Robin boundary conditions)} \\ (2.23b) \end{array}$$

$$\text{compartments} \quad \begin{cases} \lambda\xi_1 = \partial_\mu f_e \xi_1 + \partial_\eta f_e \zeta_1 + \beta_u(\phi(0) - \xi_1) & \text{(reaction kinetics at } x=0) \\ \lambda\zeta_1 = \partial_\mu g_e \xi_1 + \partial_\eta g_e \zeta_1 + \beta_v(\psi(0) - \zeta_1) \\ \lambda\xi_2 = \partial_\mu f_e \xi_2 + \partial_\eta f_e \zeta_2 + \beta_u(\phi(L) - \xi_2) & \text{(reaction kinetics at } x=L) \\ \lambda\zeta_2 = \partial_\mu g_e \xi_2 + \partial_\eta g_e \zeta_2 + \beta_v(\psi(L) - \zeta_2) \end{cases} \quad (2.23c)$$

In (2.23c) the partials of f and g evaluated at the symmetric steady-state are denoted by $\partial_\mu f_e$, $\partial_\eta f_e$, $\partial_\mu g_e$, and $\partial_\eta g_e$. In (2.23a) we defined $\Omega_u := \sqrt{(\lambda + \sigma_u)/D_u}$ and $\Omega_v := \sqrt{(\lambda + \sigma_v)/D_v}$.

Our goal is to determine all of the eigenvalues λ that are associated with nontrivial solutions to (2.23). The symmetric steady-state solution is linearly stable if all such eigenvalues satisfy $\text{Re}(\lambda) < 0$, and it is unstable if for one such eigenvalue we have $\text{Re}(\lambda) > 0$. Although our eigenvalue problem is not self-adjoint, and as such there may be a short-term transient growth of initial perturbations (cf. [23]), our numerical simulations below, confirming results from the linear stability theory, suggest that transient growth effects are unlikely to play a key role in the pattern-forming process.

Owing to the symmetry of the steady-state solution about the mid-line, the eigen-modes for (2.23) can be decomposed into two distinct classes: in-phase eigenperturbations (+) or anti-phase eigenperturbations (-), for which $\phi'_+(\frac{L}{2}) = 0 = \psi'_+(\frac{L}{2})$ or $\phi'_-(\frac{L}{2}) = 0 = \psi'_-(\frac{L}{2})$, respectively. We now derive the eigenvalue problem for these two possible eigenmodes.

For the in-phase mode, we calculate from (2.23a) and (2.23b) that

$$\begin{aligned} \phi_+(x) &= d_1^+ \frac{\cosh(\Omega_u(\frac{L}{2} - x))}{\cosh(\Omega_u L)} & \text{with} & \quad d_1^+ := \frac{\beta_u}{\beta_u + D_u \Omega_u \tanh(\Omega_u \frac{L}{2})} \xi_1, \\ \psi_+(x) &= d_2^+ \frac{\cosh(\Omega_v(\frac{L}{2} - x))}{\cosh(\Omega_v L)} & \text{with} & \quad d_2^+ := \frac{\beta_v}{\beta_v + D_v \Omega_v \tanh(\Omega_v \frac{L}{2})} \zeta_1. \end{aligned}$$

For this in-phase mode, we have $\xi_1 = \xi_2 := \xi$ and $\zeta_1 = \zeta_2 := \zeta$. Then, by using (2.23c), we obtain the 2×2 nonlinear matrix eigenvalue problem

$$M_+(\lambda) \begin{pmatrix} \xi \\ \zeta \end{pmatrix} = \begin{pmatrix} 0 \\ 0 \end{pmatrix}, \quad (2.24a)$$

where

$$M_+ := \begin{pmatrix} \lambda - \partial_\mu f_e + \beta_u \left(1 - \frac{\beta_u}{\beta_u + D_u \Omega_u \tanh(\Omega_u L/2)}\right) & -\partial_\eta f_e \\ -\partial_\mu g_e & \lambda - \partial_\eta g_e + \beta_v \left(1 - \frac{\beta_v}{\beta_v + D_v \Omega_v \tanh(\Omega_v L/2)}\right) \end{pmatrix}. \quad (2.24b)$$

Eigenvalues associated with the in-phase eigenperturbation are roots λ of $\det(M_+(\lambda)) = 0$.

Similarly, for the anti-phase mode, we calculate from (2.23a) and (2.23b) that

$$\begin{aligned} \phi_-(x) &= d_1^- \frac{\sinh(\Omega_u(\frac{L}{2} - x))}{\sinh(\Omega_u L)} & \text{with} & \quad d_1^- := \frac{\beta_u}{\beta_u + D_u \Omega_u \coth(\Omega_u \frac{L}{2})} \xi_1, \\ \psi_-(x) &= d_2^- \frac{\sinh(\Omega_v(\frac{L}{2} - x))}{\sinh(\Omega_v L)} & \text{with} & \quad d_2^- := \frac{\beta_v}{\beta_v + D_v \Omega_v \coth(\Omega_v \frac{L}{2})} \zeta_1, \end{aligned}$$

where we now label $\xi_1 = -\xi_2 := \xi$ and $\zeta_1 = -\zeta_2 := \zeta$. From (2.23c), eigenvalues λ associated with the anti-phase mode are roots of $\det(M_-(\lambda)) = 0$, where

$$M_- := \begin{pmatrix} \lambda - \partial_\mu f_e + \beta_u \left(1 - \frac{\beta_u}{\beta_u + D_u \Omega_u \coth(\Omega_u L/2)}\right) & -\partial_\eta f_e \\ -\partial_\mu g_e & \lambda - \partial_\eta g_e + \beta_v \left(1 - \frac{\beta_v}{\beta_v + D_v \Omega_v \coth(\Omega_v L/2)}\right) \end{pmatrix}. \quad (2.25)$$

By a simple scaling, the eigenvalues for the in-phase and anti-phase mode are equivalently written as the roots of $\mathcal{F}_\pm(\lambda) = 0$, where

$$\mathcal{F}_\pm(\lambda) := \frac{\det(M_\pm(\lambda))}{\det(\lambda I - DF_e)} \quad \text{with} \quad DF_e := \begin{pmatrix} \partial_\mu f_e & \partial_\eta f_e \\ \partial_\mu g_e & \partial_\eta g_e \end{pmatrix}. \quad (2.26)$$

Roots of (2.26) with $\text{Re}(\lambda) > 0$ correspond to unstable modes, while roots with $\lambda = i\lambda_i$ for $\lambda_i > 0$ yield Hopf bifurcations. To determine the number of zeroes of \mathcal{F}_\pm in the right-half plane of \mathbb{C} , denoted by $\mathcal{N}_+(\mathcal{F}_\pm)$, we numerically implement the Argument Principle given by

$$\frac{1}{2\pi i} \int_{\Gamma_R} \frac{\frac{d}{d\lambda} \mathcal{F}_\pm(\lambda)}{\mathcal{F}_\pm(\lambda)} d\lambda = \mathcal{N}_+(\mathcal{F}_\pm) - \mathcal{P}_+(\mathcal{F}_\pm), \quad (2.27)$$

where $\mathcal{P}_+(\mathcal{F}_\pm)$ is the number of poles of \mathcal{F}_\pm in $\text{Re}(\lambda) > 0$. Here we have labeled the counter-clockwise integration contour as $\Gamma_R := \{R \exp(i\varphi) | \varphi \in [-\frac{\pi}{2}, \frac{\pi}{2}]\} \cup [-iR, iR]$, with R sufficiently large so that all zeroes $\mathcal{N}_+(\mathcal{F}_\pm)$ and poles $\mathcal{P}_+(\mathcal{F}_\pm)$ are in $\text{int}(\Gamma_R)$.

Our numerical results based on (2.27) applied to $\mathcal{F}_-(\lambda)$ show for the parameter set in Fig. 3(left) that there is a unique real unstable eigenvalue for the anti-phase mode on the range $z_{P,1} < z < z_{P,2}$ between the two pitchfork points. Moreover, we numerically verified that the symmetric branch in Fig. 3(right) is linearly stable to the anti-phase mode only when ρ is below the pitchfork point.

In Fig. 4, the pitchfork points $z_{P,1}$ and $z_{P,2}$ are plotted versus ρ . From a numerical root finding of $\mathcal{F}_+(i\lambda_i) = 0$ in (2.26), together with a numerical implementation of the Argument Principle (2.27), we identify two Hopf bifurcation thresholds $z_{H,1}$ and $z_{H,2}$ for the in-phase mode, with the symmetric branch being unstable to an oscillatory instability only on the range $z_{H,1} < z < z_{H,2}$. In Fig. 4 we observe for $\rho > 75$ that the unstable oscillatory range is contained within the pitchfork range, in that the ordering $z_{P,1} < z_{H,1} < z_{H,2} < z_{P,2}$ holds. For this range of ρ , the symmetric branch is linearly stable to both in-phase and anti-phase modes on $z < z_{P,1}$ and on $z > z_{P,2}$. As a result, we predict that the symmetry-breaking bifurcation at $z_{P,1}$ and $z_{P,2}$ leads to *linearly stable asymmetric solution branches* at least locally near either $z_{P,1}$ or $z_{P,2}$. As shown in Fig. 5, this conjecture is verified in the full PDE simulations of (2.1) by the CN-RK4 IMEX method of Appendix A.

2.3 Compartments with Gierer-Meinhardt kinetics

Next, we extend our analysis to a compartmental-reaction variant of the Gierer-Meinhardt (GM) model, where the reaction kinetics are now confined to the boundaries. The original GM model, as introduced in [12] and [11] to model pattern formation in biological morphogenesis, given by

$$\begin{aligned} \partial_t u &= \varrho_0(x) + c_u \varrho_u(x) \frac{u^2}{v} + D_u \Delta u - \sigma_u u, \\ \partial_t v &= c_v \varrho_v(x) u^2 + D_v \Delta v - \sigma_v v, \end{aligned}$$

disregards that in biological tissues morphogen-producing reactions mostly occur intracellularly and on the membranes of cells. For simplicity, we illustrate our compartmental-reaction diffusion theory for the 1-D case when $\varrho_0 \equiv 0$, $c_u \varrho_u(x) \equiv 1$, and $c_v \varrho_v \equiv 1$. In our model, we restrict the reaction kinetics to the boundaries so that for the uncoupled bulk-cell model we have

$$\dot{\mu}(t) = f(\mu, \eta) := \frac{\mu^2}{\eta}, \quad \dot{\eta}(t) = g(\mu, \eta) := \mu^2. \quad (2.28)$$

Similar to the case with FN kinetics we observe that μ activates self-production and the production of η , whereas the species η only inhibits the production of μ . Hence, the GM model has a more indirect activator-inhibitor structure than the FN model, in which η also inhibits directly its own production. The uncoupled equilibrium for (2.28) is non-hyperbolic in all directions, as $DF(\mu_e, \eta_e) = 0$, where $\mu_e = 0$ and η is a constant.

To apply the bulk-cell steady-state analysis of §2.1.2 we simply identify that $g(\mu, \eta) = g_1(\mu) - g_2\eta$, where $g_1 = \mu^2$ and $g_2 = 0$. From (2.7) we get

$$A \begin{pmatrix} \eta_1^e \\ \eta_2^e \end{pmatrix} = \begin{pmatrix} (\mu_1^e)^2 \\ (\mu_2^e)^2 \end{pmatrix} \quad \text{with} \quad A = \frac{\beta_v}{\gamma_v^2 - 1} \tilde{A} := \begin{pmatrix} A_{11} & A_{12} \\ A_{12} & A_{11} \end{pmatrix}, \quad (2.29a)$$

where, by using (2.6) for \tilde{A} , we identify that

$$A_{11} = \frac{\beta_v}{\gamma_v^2 - 1} (\gamma_v \cosh(\omega_v L) - 1), \quad A_{12} = \frac{\beta_v}{\gamma_v^2 - 1} (\cosh(\omega_v L) - \gamma_v). \quad (2.29b)$$

In terms of A_{11} and A_{12} , we obtain from (2.9) after calculating A^{-1} that the nonlinear algebraic system for μ_1^e and μ_2^e reduces to

$$\begin{pmatrix} (\mu_1^e)^2 \\ (\mu_2^e)^2 \end{pmatrix} - \frac{\beta_u}{\gamma_u^2 - 1} \frac{1}{(A_{11}^2 - A_{12}^2)} \begin{pmatrix} A_{11}(\mu_1^e)^2 - A_{12}(\mu_2^e)^2 & 0 \\ 0 & -A_{12}(\mu_1^e)^2 + A_{11}(\mu_2^e)^2 \end{pmatrix} B \begin{pmatrix} \mu_1^e \\ \mu_2^e \end{pmatrix} = 0. \quad (2.30)$$

From (2.11), or equivalently from (2.30), the symmetric steady-state solution, for which $\mu_1^e = \mu_2^e = \mu_e$, is given explicitly by

$$\mu_e = \frac{a_1 (\gamma_u^2 - 1)}{b_1 \beta_u}, \quad \eta_e = \frac{\mu_e (\gamma_u^2 - 1)}{\beta_u b_1} = \frac{a_1 (\gamma_u^2 - 1)^2}{b_1^2 \beta_u^2}, \quad (2.31)$$

where $a_1 = A_{11} + A_{12}$ and b_1 are the in-phase eigenvalues of A and B given in (2.10) with $g_2 = 0$.

The linear stability of the symmetric steady-state solution is studied numerically using the methodology in §2.2.2. In contrast to the case with FN kinetics, there are no Hopf bifurcation points associated with the in-phase mode for the GM model. As a result, the symmetric steady-state cannot be destabilized by the in-phase mode. Moreover, the anti-phase mode for the linearization of the symmetric steady-state undergoes a zero-eigenvalue crossing only at any pitchfork bifurcation point $\rho = \rho_p$ that can be calculated from the nonlinear algebraic system (2.30). This symmetric steady-state is unstable to the anti-phase mode only when $\rho > \rho_p$ (as suggested by the full numerical results shown below in Fig. 7 and Fig. 8).

In Fig. 6 we plot solution branches of (2.30) for $D_u = D_v = \sigma_u = \sigma_v = 1$, $L = 1$, and $\beta_u = 0.1$, as a function of $\rho = \beta_v/\beta_u$. We observe that the symmetric branch undergoes a subcritical pitchfork bifurcation at $\rho = \rho_p \approx 13.10$. The emerging unstable asymmetric equilibria undergo a secondary fold bifurcation at $\rho_f \approx 5.59$. The asymmetric branches are found to be linearly stable for $\rho > \rho_f$. As a result, we conclude that linearly stable asymmetric patterns occur even when $D_u = D_v$.

From Fig. 6, the bifurcation structure of equilibria for (2.30) exhibits a hysteresis structure. As shown in Fig. 7 for $\rho = 4$ and $\rho = 8$, for an initial condition near the symmetric branch when $\rho \in [1, \rho_p)$, the full PDE simulations of (2.1) by the CN-RK4 IMEX method of Appendix A verifies the convergence to the symmetric steady-state branch. In contrast, the full numerical results shown in Fig. 8(left) for $\rho > \rho_f$ confirms that for an initial condition near the stable asymmetric solution branch the time-dependent solution converges to the asymmetric branch. Moreover, in Fig. 8(right) when $\rho = 25 > \rho_p$ an initial condition near the unstable symmetric branch is shown to converge to the asymmetric solution branch.

For the classical GM RD model without reaction compartments, it is well-known from a standard Turing analysis that stable spatially non-uniform solutions can only occur when the diffusivity ratio D_v/D_u is sufficiently large. In our compartmental-reaction diffusion model, in

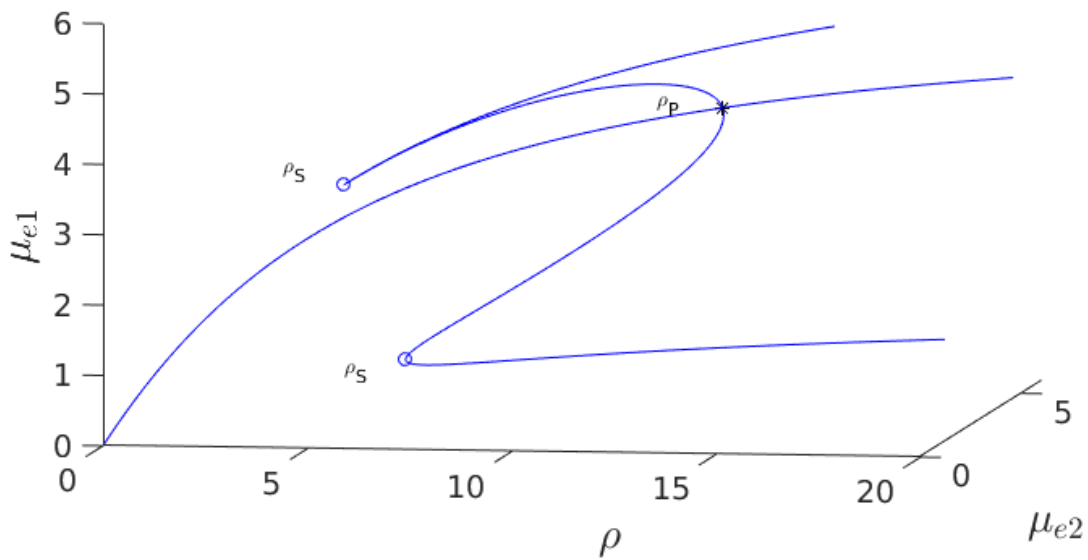


Figure 6: 3-D bifurcation diagram for μ_{e1} and μ_{e2} with bifurcation parameter $\rho = \beta_v/\beta_u$ for steady-states of the GM compartmental-reaction diffusion system as computed from (2.30) using MatCont [5]. There is a subcritical pitchfork bifurcation from the symmetric steady-state at $\rho_p \approx 13.09728$, with (secondary) fold point bifurcations occurring on the asymmetric branches at $\rho_f \approx 5.59447$. For $\rho < \rho_p$ the symmetric steady-state is linearly stable, while for $\rho > \rho_f$ the asymmetric branches are linearly stable. Parameters: $D_u = D_v = 1, \sigma_u = \sigma_v = 1, L = 1$, and $\beta_u = 0.1$.

Table 1 we show that asymmetric solution branches bifurcate from the symmetric branch even when $D_v < D_u$. As seen from this table, the required binding rate ratio threshold ρ_p increases as D_v/D_u decreases. Furthermore, the extent of the hysteresis, as measured by the values of $\rho_p - \rho_f$ and $\mu_1^e - \mu_2^e$, becomes larger as D_v/D_u decreases. Regarding the dependence of the hysteresis on the binding rates β_u and $\beta_v = \rho\beta_u$, Table 2 shows that if $\beta_u \geq 0.35$ there is now a supercritical pitchfork bifurcation from the symmetric branch and the hysteresis structure disappears.

D_v/D_u	0.4	0.5	0.6	0.7	0.8	0.9	1
ρ_p	> 100	52.18853	26.86097	19.71589	16.34470	14.38188	13.09728
μ_e		4.83783	4.60295	4.43970	4.31969	4.22776	4.15511
ρ_f		9.33646	7.71235	6.82347	6.26265	5.87653	5.59447
μ_1^e		4.24548	4.03936	3.89609	3.79078	3.71011	3.64635
μ_2^e		0.70991	0.67544	0.65148	0.63387	0.620385	0.60972
D_v/D_u	1.1	1.2	1.3	1.4	1.5	1.6	
ρ_p	14.38188	11.51761	10.99734	10.58334	10.24607	...	
μ_e	4.22776	4.04759	4.00670	3.97186	3.94181		
ρ_f	5.87653	5.20997	5.07306	4.96011	4.86535		
μ_1^e	3.71011	3.55200	3.51612	3.48554	3.45917		
μ_2^e	0.62038	0.59395	0.58795	0.58283	0.57842		

Table 1: Numerical values (rounded to 5th decimal place) of the subcritical pitchfork bifurcation point ρ_p for the symmetric branch and the two fold bifurcation points ρ_f along the asymmetric branches. Bifurcation values for the symmetric (μ_e) and one of the asymmetric (μ_1^e, μ_2^e) solution branches are listed. As the ratio D_v/D_u decreases the range of ρ where hysteresis occurs increases. Parameters: $D_u = 1, \sigma_u = \sigma_v = 1, L = 1$, and $\beta_u = 0.1$.

β_u	0.05	0.1	0.15	0.2	0.25	0.3	0.35
ρ_p	20.44213	13.09728	11.42015	11.59667	13.33412	17.91935	33.18867
μ_e	7.05336	4.15511	3.21380	2.76056	2.50167	2.33930	2.23156
ρ_f	4.69415	5.59447	6.82631	8.63523	11.58010	17.27125	-
μ_1^e	3.82650	3.64635	3.45845	3.25882	3.03717	2.76171	-
μ_2^e	0.32048	0.60972	0.87895	1.13950	1.40694	1.71692	-

Table 2: Numerical values (rounded to 5th decimal place) of the subcritical (or supercritical) pitchfork bifurcation point ρ_p , the two fold bifurcation points ρ_f , and the corresponding values for the symmetric (μ_e) and one of the asymmetric (μ_1^e, μ_2^e) solution branches. As β_u increases from 0.05, the range of ρ where hysteresis occurs decreases, until a supercritical pitchfork bifurcation arises when $\beta_u \approx 0.35$. Parameters: $D_u = D_v = 1, \sigma_u = \sigma_v = 1, L = 1$.

2.4 Compartments with Rauch-Millonas kinetics

We now briefly show that linearly stable asymmetric patterns can occur for a compartmental-reaction diffusion model using the generic intracellular reaction kinetics proposed in [44]

$$\begin{aligned}\dot{\mu} &= f(\mu, \eta) := c_u - q_u\mu + \frac{\alpha_1^u\mu}{\gamma_1^u + \mu} - \frac{\alpha_2^u\mu\eta}{\gamma_2^u + \mu} \\ \dot{\eta} &= g(\mu, \eta) := c_v + w_v\mu - q_v\eta,\end{aligned}\tag{2.32}$$

where we identify $g_1(\mu) = c_v + w_v\mu$ and $g_2 = q_v$. This kinetic model was proposed in [44] as a simplified universal description for signal transduction kinetics in cells.

Owing to the special form of $g(\mu, \eta)$, we can readily implement the steady-state theory of §2.1.2 when the kinetics (2.32) are restricted to the domain boundaries. Parameters are chosen as in [44] to ensure that the uncoupled dynamics (2.32) has a stable equilibrium point.

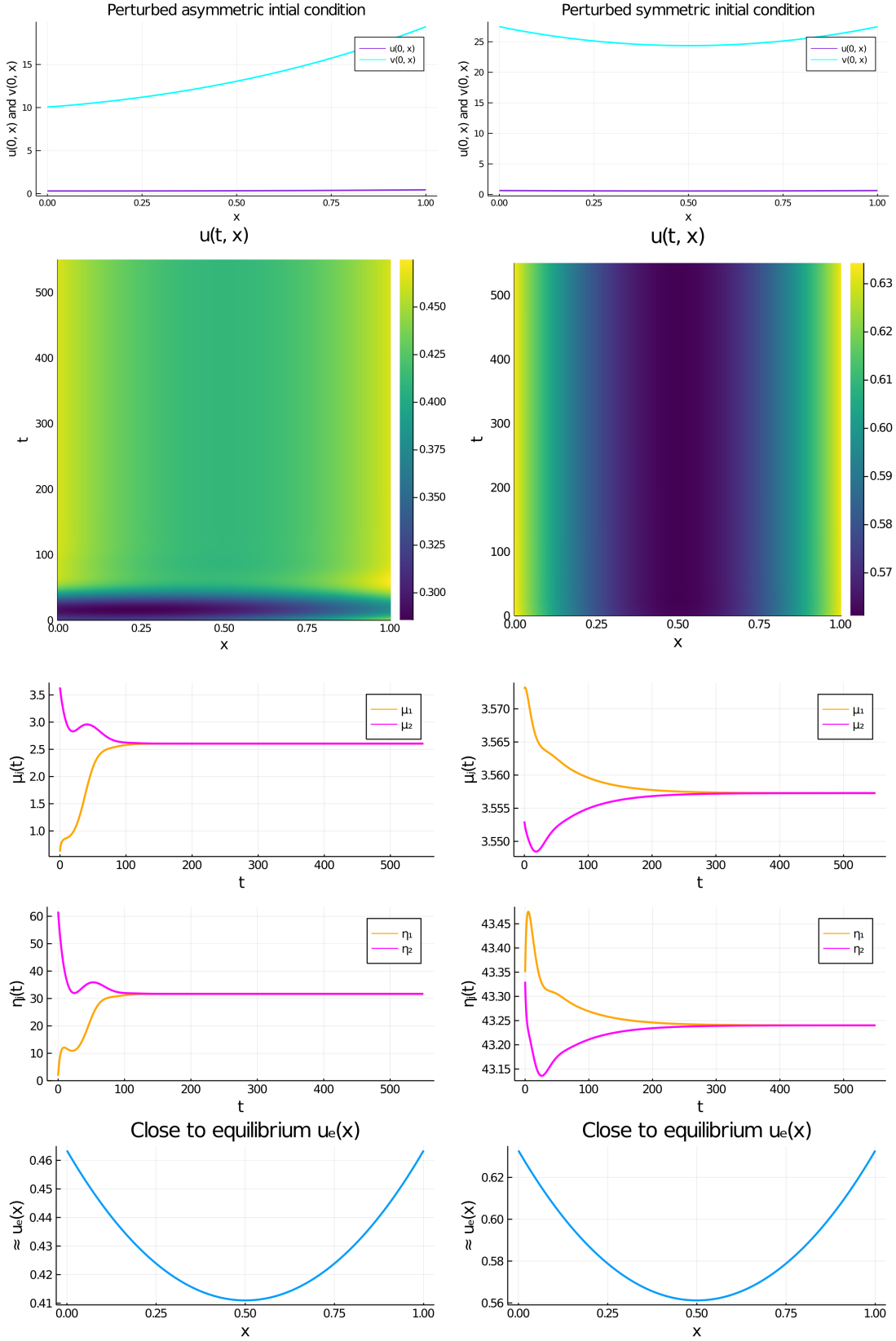


Figure 7: Full numerical computations of (2.1) by the CN-RK4 IMEX method of Appendix A for GM kinetics. Left: convergence to the symmetric branch for $\rho = 4$ starting close to the symmetric branch. Right: convergence to the symmetric branch for $\rho = 8$ and starting near the symmetric branch. The remaining parameter values are as in the caption to Fig. 6.

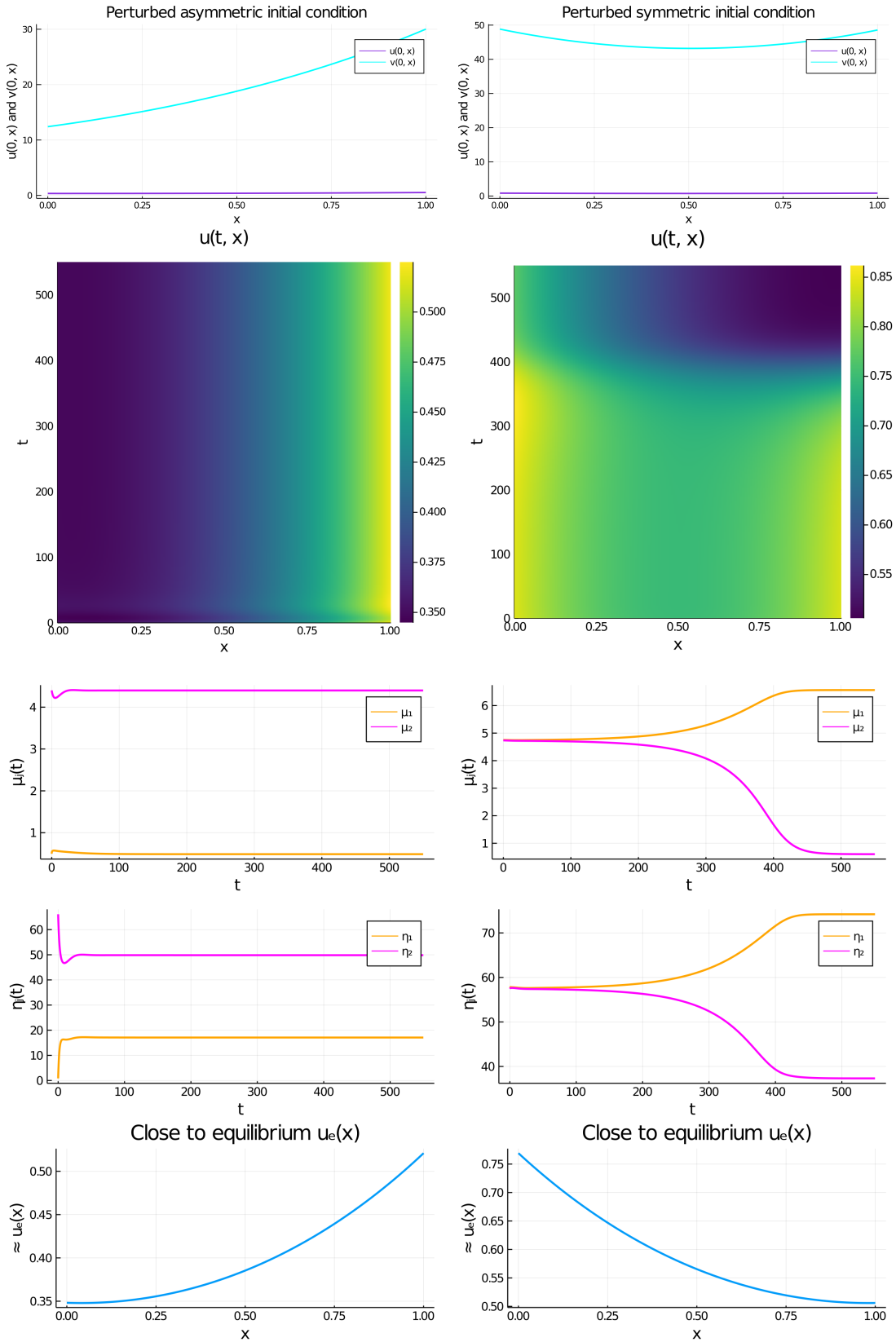


Figure 8: Full numerical computations of (2.1) by the CN-RK4 IMEX method for GM kinetics. Left: convergence to the asymmetric branch for $\rho = 8$ starting near one of the stable asymmetric branches for $\rho > \rho_f$. Right: convergence to an asymmetric branch for $\rho = 25$ starting close to the symmetric branch with perturbation toward the respective asymmetric branch. The remaining parameter values are as in the caption to Fig. 6.

With ω_v or the binding rate ratio $\rho = \beta_v/\beta_u$ as bifurcation parameters, we use MatCont [5] to numerically compute steady-states of the bulk-cell model. With the other parameters similar to those in [44], in Fig. 9(right) we observe that asymmetric patterns do emerge from the symmetric solution branch as ρ exceeds a threshold. Pitchfork bifurcations in w_v also occur (see Fig. 9(left)), and they correspond as before to a zero-eigenvalue crossing of the anti-phase perturbation of the symmetric steady-state. The full-time dependent numerical computations shown in Fig. 10 confirms the existence of stable asymmetric steady-state patterns.

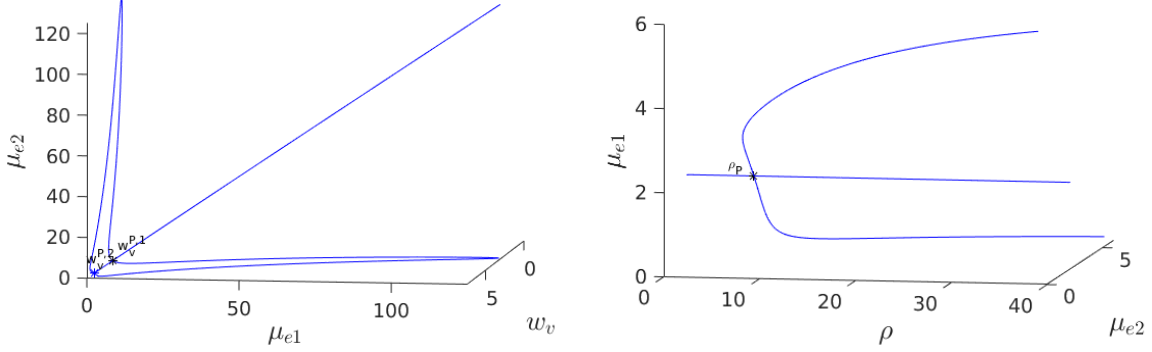


Figure 9: 3-D bifurcation diagrams using MatCont [5] for the two-cell compartmental-reaction diffusion system with Rauch-Millonas kinetics (2.32): Left: Plot of μ_1^e showing that asymmetric steady-states occur inside the degenerate pitchfork bubble delimited by $w_v^{P,1} \approx 6.67610$ and $w_v^{P,2} \approx 7.28516$ when $\rho = \beta_v/\beta_u = 7$. Right: Supercritical pitchfork bifurcation from the symmetric branch occurs when $w_v^{P,2} \approx 7.28516$. Linearly stable asymmetric branches occur past this threshold in ρ . Parameters: $D_u = D_v = 1, \sigma_u = \sigma_v = 0.01, L = 1, c_u = c_v = 1, q_u = 1/100, q_v = 7, \alpha_1^u = 600, \alpha_2^u = 6, \gamma_1^u = 100, \gamma_2^u = 1/10$, and $\beta_u = 0.3$.

3 A Periodic Compartmental-Reaction Diffusion Model

We now extend the two-compartment model to allow for a periodic array of identical reaction compartments in 1-D. Our goal is to investigate symmetry-breaking behavior from a symmetric steady-state for this extended model. For a periodic chain of compartments there can be multiple possible modes of instability of the symmetric steady-state.

In our formulation, we consider a periodic chain of a fixed length $nL, n \in \mathbb{N} \setminus \{0, 1\}, L > 0$, with compartments centered at $x_j = \frac{(2j-1)}{2}L$ for $j \in \{1, \dots, n\}$, so that for $x \in \mathbb{R} \setminus (nL \cdot \mathbb{Z})$ we have the following bulk-cell system on the domain $0 < x < nL$ (see Fig. 11 for a schematic):

$$\text{bulk} \quad \begin{cases} \partial_t u = D_u \partial_{xx} u - \sigma_u u, & t \in (0, \infty), x \in (0, nL) \setminus \bigcup_{j=1}^n \{x_j\} \\ \partial_t v = D_v \partial_{xx} v - \sigma_v v, & t \in (0, \infty), x \in (0, nL) \setminus \bigcup_{j=1}^n \{x_j\} \end{cases} \quad (3.33a)$$

$$\text{bulk boundary} \quad \begin{cases} u(t, 0) = u(t, nL), & v(t, 0) = v(t, nL) \quad (\text{periodic BC}) \\ \partial_x u(t, 0) = \partial_x u(t, nL), & \partial_x v(t, 0) = \partial_x v(t, nL) \end{cases} \quad (3.33b)$$

$$\text{reaction fluxes} \quad \begin{cases} [D_u \partial_x u]|_{x=x_j} = \beta_u (u(t, x_j) - \mu_j(t)) & (\text{cell jump conditions}) \\ [D_v \partial_x v]|_{x=x_j} = \beta_v (v(t, x_j) - \eta_j(t)) \end{cases} \quad (3.33c)$$

$$\text{compartments} \quad \begin{cases} \dot{\mu}_j = f(\mu_j, \eta_j) + [D_u \partial_x u]|_{x=x_j} & (\text{reaction kinetics at } x = x_j) \\ \dot{\eta}_j = g(\mu_j, \eta_j) + [D_v \partial_x v]|_{x=x_j}, \end{cases} \quad (3.33d)$$

for $j = \{1, \dots, n\}$. Here for any function \mathcal{F} we have defined $[\mathcal{F}]|_{x=\tilde{x}} := \mathcal{F}(\tilde{x}^+) - \mathcal{F}(\tilde{x}^-)$.

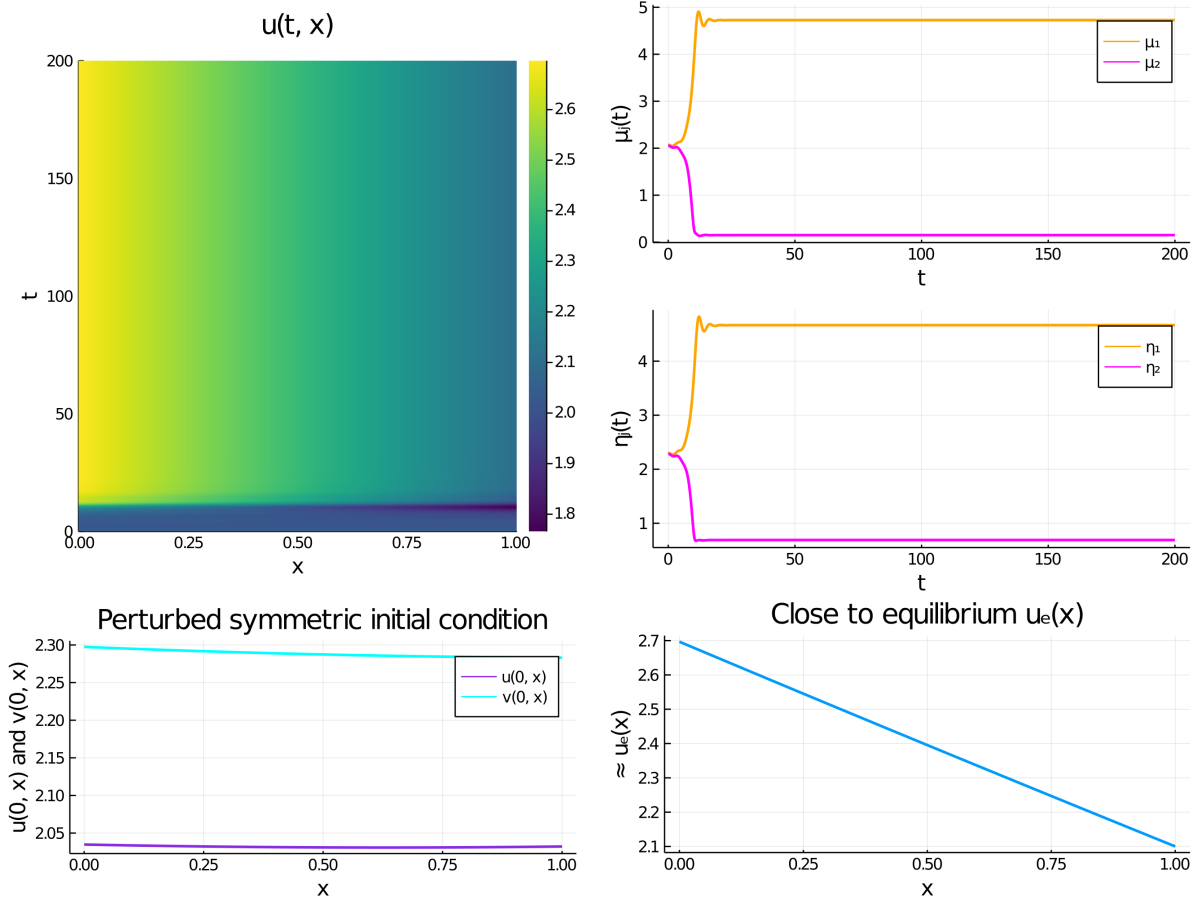


Figure 10: Full numerical computations of (2.1) by the CN-RK4 IMEX method of Appendix A for Rauch-Millonas kinetics (2.32). For $\rho = 15$ and $w_v = w_v^{P,2} \approx 7.28516$, and with an initial condition near the unstable symmetric branch (see Fig. 9(right)), the time-dependent solution converges to a stable asymmetric pattern. Parameters are as in the caption of Fig. 9.

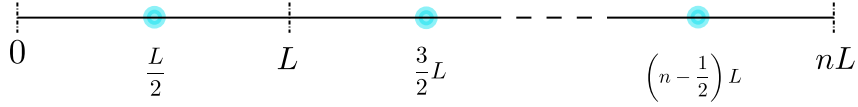


Figure 11: The periodic compartmental-reaction diffusion model on $[0, nL]$ with compartments centered at the blue dots. Two bulk diffusing species provide the inter-compartment coupling.

3.1 Compartments with general reaction kinetics

We will first construct a symmetric steady-state solution for (3.33) and we will analyze the linear stability of this steady-state by using a Floquet-based approach. Owing to the complexity of (3.33), we will not construct asymmetric steady-states of (3.33).

3.1.1 Symmetric steady-state and the linear stability problem

To construct a symmetric steady-state u_e, v_e for (3.33) we need only consider the *fundamental domain* $[0, L]$ upon which we impose periodic boundary conditions

$$u_e(0) = u_e(L), \quad v_e(0) = v_e(L), \quad \partial_x u_e(0) = \partial_x u_e(L), \quad \partial_x v_e(0) = \partial_x v_e(L). \quad (3.34)$$

The symmetric steady-state is obtained by a periodic extension to the entire chain.

To represent the steady-states in the bulk, we introduce the periodic Green function $G_\omega(x)$.

Definition 3.1. *The periodic Green function on $[0, L]$ with singularity at $x = \frac{L}{2}$ is the solution of*

$$\partial_{xx} G_\omega - \omega^2 G_\omega = -\delta(x - \frac{L}{2}), \quad x \in [0, L]; \quad G_\omega(0) = G_\omega(L), \quad \partial_x G_\omega(0) = \partial_x G_\omega(L), \quad (3.35a)$$

$$G_\omega(\frac{L^+}{2}) = G_\omega(\frac{L^-}{2}), \quad \partial_x G_\omega(\frac{L^+}{2}) - \partial_x G_\omega(\frac{L^-}{2}) = -1. \quad (3.35b)$$

The solution to (3.35) is readily calculated as

$$G_\omega(x) = \begin{cases} \frac{1}{2\omega} \coth\left(\frac{\omega L}{2}\right) \cosh\left(\omega\left(\frac{L}{2} - x\right)\right) - \frac{1}{2\omega} \sinh\left(\omega\left(\frac{L}{2} - x\right)\right), & x \in [0, \frac{L}{2}], \\ \frac{1}{2\omega} \coth\left(\frac{\omega L}{2}\right) \cosh\left(\omega\left(\frac{L}{2} - x\right)\right) + \frac{1}{2\omega} \sinh\left(\omega\left(\frac{L}{2} - x\right)\right), & x \in [\frac{L}{2}, L], \end{cases} \quad (3.36)$$

where we identify that $G_\omega(L/2) = \frac{1}{2\omega} \coth(\omega L/2)$.

Upon defining $\omega_u := \sqrt{\sigma_u/D_u}$ and $\omega_v := \sqrt{\sigma_v/D_v}$ the bulk steady-state solutions satisfying (3.33a) and (3.33c) on the fundamental domain $[0, L]$ with periodic boundary conditions (3.34) are

$$\begin{aligned} u_e(x) &= c_1 \frac{G_{\omega_u}(x)}{G_{\omega_u}(L/2)} & \text{with} & \quad c_1 := \frac{\beta_u}{\beta_u + 2D_u \omega_u \tanh(\omega_u L/2)} \mu_e, \\ v_e(x) &= c_2 \frac{G_{\omega_v}(x)}{G_{\omega_v}(L/2)} & \text{with} & \quad c_2 := \frac{\beta_v}{\beta_v + 2D_v \omega_v \tanh(\omega_v L/2)} \eta_e. \end{aligned} \quad (3.37)$$

Finally, upon substituting (3.37) into the steady-state of the intra-compartment dynamics (3.33d) we obtain that μ_e and η_e satisfy the nonlinear algebraic system

$$f(\mu_e, \eta_e) = \frac{2D_u \omega_u \beta_u}{\beta_u \coth(\omega_u L/2) + 2D_u \omega_u} \mu_e, \quad g(\mu_e, \eta_e) = \frac{2D_v \omega_v \beta_v}{\beta_v \coth(\omega_v L/2) + 2D_v \omega_v} \eta_e. \quad (3.38)$$

In this way, for a given reaction-kinetics, we can determine the symmetric equilibrium (μ_e, η_e) by a numerical root finding on (3.38).

We now formulate and study the linear stability problem for the symmetric steady-state solution branch. For the linear stability analysis we perturb the symmetric steady-state by introducing $u(t, x) = u_e(x) + \phi(x)e^{\lambda t}$, $v(t, x) = v_e(x) + \psi(x)e^{\lambda t}$, $\mu_j(t) = \mu_e + \xi_j e^{\lambda t}$, $\eta = \eta_e + \zeta_j e^{\lambda t}$,

where $|\phi| \ll 1$, $|\psi| \ll 1$, $|\xi_j| \ll 1$ and $|\zeta_j| \ll 1$ for $j \in \{1, 2\}$, into (3.33) and linearizing. This yields the linearized eigenvalue problem

$$\text{bulk} \quad \begin{cases} \partial_{xx}\phi - \Omega_u^2\phi = 0, & x \in (0, nL) \setminus \bigcup_{j=1}^n \{x_j\} \\ \partial_{xx}\psi - \Omega_v^2\psi = 0, & x \in (0, nL) \setminus \bigcup_{j=1}^n \{x_j\} \end{cases} \quad (3.39a)$$

$$\text{bulk boundary} \quad \begin{cases} \phi(0) = \phi(nL), & \psi(0) = \psi(nL) & \text{(periodic BC)} \\ \partial_x\phi(0) = \partial_x\phi(nL), & \partial_x\psi(0) = \partial_x\psi(nL) \end{cases} \quad (3.39b)$$

$$\text{reaction fluxes} \quad \begin{cases} [D_u\partial_x\phi]|_{x=x_j} = \beta_u(\phi(x_j) - \xi_j) & \text{(cell jump conditions)} \\ [D_v\partial_x\psi]|_{x=x_j} = \beta_v(\psi(x_j) - \zeta_j) \end{cases} \quad (3.39c)$$

$$\text{compartments} \quad \begin{cases} \lambda\xi_j = \partial_\mu f_e \xi_j + \partial_\eta f_e \zeta_j + [D_u\partial_x\phi]|_{x=x_j} & \text{(reaction kinetics at } x = x_j) \\ \lambda\zeta_j = \partial_\mu g_e \xi_j + \partial_\eta g_e \zeta_j + [D_v\partial_x\psi]|_{x=x_j} \end{cases} \quad (3.39d)$$

for $j \in \{1, \dots, n\}$. Here we have defined $\Omega_u := \sqrt{(\lambda + \sigma_u)/D_u}$ and $\Omega_v := \sqrt{(\lambda + \sigma_v)/D_v}$.

To study this eigenvalue problem, it is convenient to use a Floquet-based approach where we consider the *fundamental cell problem* on $[0, L]$ and impose a Floquet-type boundary condition:

$$\text{bulk} \quad \begin{cases} \partial_{xx}\phi - \Omega_u^2\phi = 0, & x \in (0, L) \setminus \{\frac{L}{2}\} \\ \partial_{xx}\psi - \Omega_v^2\psi = 0, & x \in (0, L) \setminus \{\frac{L}{2}\} \end{cases} \quad (3.40a)$$

$$\text{bulk boundary} \quad \begin{cases} \phi(0) = Z\phi(L), & \psi(0) = Z\psi(L) & \text{(Floquet BC)} \\ \partial_x\phi(0) = Z\partial_x\phi(L), & \partial_x\psi(0) = Z\partial_x\psi(L) \end{cases} \quad (3.40b)$$

$$\text{reaction fluxes} \quad \begin{cases} [D_u\partial_x\phi]|_{x=\frac{L}{2}} = \beta_u(\phi(\frac{L}{2}) - \xi) & \text{(cell jump conditions)} \\ [D_v\partial_x\psi]|_{x=\frac{L}{2}} = \beta_v(\psi(\frac{L}{2}) - \zeta) \end{cases} \quad (3.40c)$$

$$\text{intracellular} \quad \begin{cases} \lambda\xi = \partial_\mu f_e \xi + \partial_\eta f_e \zeta + [D_u\partial_x\phi]|_{x=\frac{L}{2}} & \text{(reaction kinetics at } x = \frac{L}{2}) \\ \lambda\zeta = \partial_\mu g_e \xi + \partial_\eta g_e \zeta + [D_v\partial_x\psi]|_{x=\frac{L}{2}}, \end{cases} \quad (3.40d)$$

for $Z \in \mathbb{C}$. Upon using translational invariance, we get the chain

$$\phi(0) = Z\phi(L) = Z^2\phi(2L) = \dots = Z^n\phi(nL),$$

so that in order to satisfy $\phi(0) = \phi(nL)$, we must have that

$$Z^n = 1 \quad \Leftrightarrow \quad Z_k = e^{2\pi ik/n}, \quad \text{for } k \in \{0, \dots, n-1\}. \quad (3.41)$$

Such a Floquet-inspired approach to more readily derive the eigenvalue equation in this periodic setting has been used previously in other contexts. In §3 of [25] a similar approach was used to analyze the stability of a periodic pattern of localized hot-spots or “spikes” for a reaction-diffusion model of urban crime. It was also used in §5.2 of [15] to analyze the linear stability of a compartment-reaction diffusion model with a periodic array of compartments, but with only one-bulk diffusing species.

Remark 3.1. *Since $Z = 1$ when $k = 0$, the mode $k = 0$ represents in-phase perturbations of the symmetric steady-state. There are $n - 1$ other possible modes of instability, which we shall refer to as “asymmetric modes”. For the special case $n = 2$, we have $Z_1 = -1$ and $\phi(0) = -\phi(L)$, and we refer to this mode as the anti-phase mode.*

In order to derive an explicit formula for the eigenvalues λ of (3.40) for a given Z , we must first introduce the the *quasi-periodic* Green function $G_{\Omega, Z}$.

Definition 3.2. The quasi-periodic Green function on the fundamental domain $[0, L]$ with singularity at $x = \frac{L}{2}$ is the solution of

$$\partial_{xx}G_{\Omega,Z} - \Omega^2 G_{\Omega,Z} = -\delta(x - \frac{L}{2}), \quad x \in [0, L], \quad (3.42a)$$

$$G_{\Omega,Z}(0) = ZG_{\Omega,Z}(L), \quad \partial_x G_{\Omega,Z}(0) = Z\partial_x G_{\Omega,Z}(L), \quad (3.42b)$$

$$G_{\Omega,Z}(\frac{L^+}{2}) = G_{\Omega,Z}(\frac{L^-}{2}), \quad \partial_x G_{\Omega,Z}(\frac{L^+}{2}) - \partial_x G_{\Omega,Z}(\frac{L^-}{2}) = -1. \quad (3.42c)$$

Upon satisfying the continuity and jump conditions in (3.42c), the explicit solution to (3.42a) can be written in terms of two constants A_Ω and B_Ω as

$$G_{\Omega,Z}(x) = \begin{cases} A_\Omega \cosh(\Omega(\frac{L}{2} - x)) + B_\Omega \sinh(\Omega(\frac{L}{2} - x)), & x \in [0, \frac{L}{2}], \\ A_\Omega \cosh(\Omega(\frac{L}{2} - x)) + (\frac{1}{\Omega} + B_\Omega) \sinh(\Omega(\frac{L}{2} - x)), & x \in [\frac{L}{2}, L]. \end{cases} \quad (3.43)$$

Then, by satisfying the quasi-periodic boundary conditions in (3.42a), we obtain a matrix problem

$$E \begin{pmatrix} A_\Omega \\ B_\Omega \end{pmatrix} = \frac{Z}{\Omega} \begin{pmatrix} -\sinh(\frac{\Omega L}{2}) \\ \cosh(\frac{\Omega L}{2}) \end{pmatrix}, \quad \text{with} \quad E := \begin{pmatrix} (1-Z) \cosh(\frac{\Omega L}{2}) & (1+Z) \sinh(\frac{\Omega L}{2}) \\ (1+Z) \sinh(\frac{\Omega L}{2}) & (1-Z) \cosh(\frac{\Omega L}{2}) \end{pmatrix}.$$

Next, we invert the matrix E by using $\det(E) = 1 - 2Z \cosh(\Omega L) + Z^2$ and $Z + 1/Z = 2\text{Re}(Z)$ when $|Z|^2 = 1$. This determines A_Ω and B_Ω as

$$\begin{pmatrix} A_\Omega \\ B_\Omega \end{pmatrix} = \frac{1}{2\Omega (\text{Re}(Z) - \cosh(\Omega L))} \begin{pmatrix} -\sinh(\Omega L) \\ -Z + \cosh(\Omega L) \end{pmatrix}. \quad (3.44)$$

The explicit formula for $G_{\Omega,Z}$ immediately follows from (3.44) and (3.43). By setting $x = L/2$ in (3.43) and using (3.44), we get

$$G_{\Omega,Z}\left(\frac{L}{2}\right) = \frac{\sinh(\Omega L)}{2\Omega [\cosh(\Omega L) - \text{Re}(Z)]}. \quad (3.45)$$

As a remark, for $Z = 1$ in (3.43) and (3.44) we recover the periodic Green function in (3.36).

In terms of this Green function, the solution to (3.40a)–(3.40c) is

$$\begin{aligned} \phi(x) &= d_1 \frac{G_{\Omega_u,Z}(x)}{G_{\Omega_u,Z}(L/2)} & \text{with} \quad d_1 &= \frac{\beta_u G_{\Omega_u,Z}(L/2)}{\beta_u G_{\Omega_u,Z}(L/2) + D_u} \xi, \\ \psi(x) &= d_2 \frac{G_{\Omega_v,Z}(x)}{G_{\Omega_v,Z}(L/2)} & \text{with} \quad d_2 &= \frac{\beta_v G_{\Omega_v,Z}(L/2)}{\beta_v G_{\Omega_v,Z}(L/2) + D_v} \zeta. \end{aligned}$$

Finally, from (3.40d) we obtain an explicit nonlinear matrix eigenvalue problem for determining λ

$$M_Z(\lambda) \begin{pmatrix} \xi \\ \zeta \end{pmatrix} = \begin{pmatrix} 0 \\ 0 \end{pmatrix}, \quad (3.46a)$$

$$\text{where} \quad M_Z(\lambda) := \begin{pmatrix} \lambda - \partial_\mu f_e + \frac{\beta_u D_u}{\beta_u G_{\Omega_u,Z}(L/2) + D_u} & -\partial_\eta f_e \\ -\partial_\mu g_e & \lambda - \partial_\eta g_e + \frac{\beta_v D_v}{\beta_v G_{\Omega_v,Z}(L/2) + D_v} \end{pmatrix}. \quad (3.46b)$$

In calculating $G_{\Omega_u,Z}(L/2)$ and $G_{\Omega_v,Z}(L/2)$ from (3.45) we recall that $\Omega_u = \sqrt{(\lambda + \sigma_u)/D_u}$ and $\Omega_v = \sqrt{(\lambda + \sigma_v)/D_v}$.

It follows that λ is an eigenvalue of the linearization (3.39) if and only if for a given $Z = Z_k$ with $k \in \{0, \dots, n-1\}$, we have $\det(M_Z(\lambda)) = 0$. To determine zero-eigenvalue crossings for a given mode Z_k when a parameter, such as the binding rate ratio $\rho = \beta_v/\beta_u$, is varied, we must simultaneously solve $\det(M_{Z_k}(\lambda)) = 0$ together with the nonlinear algebraic system (3.38) for the steady-state to identify the bifurcation point. Such zero-eigenvalue crossings for mode Z_k correspond to symmetry-breaking bifurcations from the symmetric steady-state.

We now clarify how the Floquet modes Z_k are related to the form of the perturbation near each cell centered at $x = x_j = (j - 1/2)L$ for $j \in \{1, \dots, n\}$, whenever we have a zero-eigenvalue crossing $\lambda = 0$ obtained from setting $\det(M_{Z_k}(0)) = 0$ for any $k \in \{0, \dots, n-1\}$. Labeling $\phi_{\text{cell},j,k} := \phi((j - 1/2)L)$, we have by translation invariance that $\phi_{\text{cell},j,k} = Z_k^{j-1} \phi(L/2)$ when $Z = Z_k$. In this way, we can define a vector characterizing the perturbation of the symmetric steady-state u_e at the cell locations by

$$\phi_{\text{cell},k} := \begin{pmatrix} \phi_{\text{cell}1,k} \\ \phi_{\text{cell}2,k} \\ \vdots \\ \phi_{\text{cell}n,k} \end{pmatrix} = \begin{pmatrix} 1 \\ Z_k \\ \vdots \\ Z_k^{n-1} \end{pmatrix} \phi(L/2). \quad (3.47)$$

In a similar way, we can identify for (3.39) in terms of the fundamental cell variables that $\psi_{\text{cell},j,k} := \psi((j - 1/2)L) = Z_k^{j-1} \psi(L/2)$, $\xi_{jk} = Z_k^{j-1} \xi$, and $\zeta_{jk} = Z_k^{j-1} \zeta$ for $j \in \{1, \dots, n\}$.

Since $G_{\Omega, Z_k}(L/2)$ from (3.45) and, consequently, $M_{Z_k}(\lambda)$ in (3.46) are real-valued when λ is real, we conclude that $\phi(L/2)$ is real-valued when λ is real. By taking the real and imaginary parts of (3.47) we conclude that

$$\phi_{\text{cell},k} \in \text{span}\{\mathbf{v}_{ck}, \mathbf{v}_{sk}\}, \quad \mathbf{v}_{ck} := \begin{pmatrix} 1 \\ \vdots \\ \cos\left(\frac{2\pi(j-1)k}{n}\right) \\ \vdots \\ \cos\left(\frac{2\pi(n-1)k}{n}\right) \end{pmatrix}, \quad \mathbf{v}_{sk} := \begin{pmatrix} 0 \\ \vdots \\ \sin\left(\frac{2\pi(j-1)k}{n}\right) \\ \vdots \\ \sin\left(\frac{2\pi(n-1)k}{n}\right) \end{pmatrix}. \quad (3.48)$$

When $n = 2$, we have either $Z_0 = 1$ or $Z_0 = -1$. For the in-phase mode $Z_0 = 1$, we have $\mathbf{v}_{s0} = \mathbf{0}$, and so (3.48) yields $\phi_{\text{cell},0} \in \text{span}\{\mathbf{v}_{c0}\} = \text{span}\{(1, 1)^T\}$. Likewise, for the anti-phase mode $Z_0 = -1$ we have $\phi_{\text{cell},1} \in \text{span}\{\mathbf{v}_{c1}\} = \text{span}\{(1, -1)^T\}$. For any $n \geq 2$, we always have the in-phase mode $Z_0 = 1$ for which $\phi_{\text{cell},0} \in \text{span}\{\mathbf{v}_{c0}\} = \text{span}\{(1, \dots, 1)^T\}$.

Now suppose that $n > 2$ is even. Then, since $Z_{n/2} = e^{i\pi} = -1$, we will have a zero-eigenvalue crossing for an anti-phase perturbation $\phi_{\text{cell},k/2} \in \text{span}\{(1, -1, \dots, 1, -1)^T\}$, whenever there is a bifurcation parameter for which $\det(M_{Z_{n/2}}(0)) = 0$. Furthermore, since $\text{Re}Z_k = \text{Re}Z_{n-k}$ and, consequently, $M_{Z_k}(\lambda) = M_{Z_{n-k}}(\lambda)$ in (3.46) for $k \in \{1, \dots, \frac{n}{2} - 1\}$, we conclude that the bifurcation parameter thresholds for which $\det(M_{Z_k})(0) = 0$ and $\det(M_{Z_{n-k}})(0) = 0$ are identical. As a result, we have $n/2 - 1$ “degenerate” asymmetric modes when $n > 2$ is even. Since $\mathbf{v}_{ck} = \mathbf{v}_{c(n-k)}$ and $\mathbf{v}_{sk} = -\mathbf{v}_{s(n-k)}$ for $k \in \{1, \dots, \frac{n}{2} - 1\}$, we conclude from (3.48) that $\phi_{\text{cell},k} \in \text{span}\{\mathbf{v}_{ck}, \mathbf{v}_{sk}\}$ for $k \in \{1, \dots, \frac{n}{2} - 1\}$.

In contrast, for $n \geq 3$ with n odd, there is no anti-phase mode and there are exactly $\frac{n+1}{2} - 1$ possible degenerate asymmetric modes for which the bifurcation parameter thresholds are determined from setting $\det(M_{Z_k})(0) = 0$ for $k \in \{1, \dots, \frac{n+1}{2} - 1\}$. We again conclude from (3.48) that $\phi_{\text{cell},k} \in \text{span}\{\mathbf{v}_{ck}, \mathbf{v}_{sk}\}$ for $k \in \{1, \dots, \frac{n+1}{2} - 1\}$. In particular, when $n = 3$, we conclude that at the zero-eigenvalue crossing for either $Z = Z_1$ or $Z = Z_2$ there is a two-dimensional eigenspace for the vector $\phi_{\text{cell},1}$ of cell perturbations given by the plane $(1, 1, 1)^T \phi_{\text{cell},1} = 0$.

3.2 Two Compartments with $g(\mu, \eta) = g_1(\mu) - g_2\eta$

The analysis so far for the periodic problem has focused on constructing the symmetric steady-state and formulating the linear stability problem so as to readily detect symmetry-breaking bifurcation points for any $n \geq 2$ and arbitrary intra-compartment reactions f and g .

In this subsection, we briefly focus on the two-compartment case $n = 2$ when $g(\mu, \eta) = g_1(\mu) - g_2\eta$ with an aim of constructing both symmetric and asymmetric branches of equilibria. Since the analysis is similar to that in §2.1.2 we only briefly highlight it here.

For $n = 2$ compartments, the steady-state for u_e has the form

$$u_e(x) = \begin{cases} A_1 \sinh(\omega_u(\frac{L}{2} - x)) + A_2 \sinh(\omega_u x), & x \in [0, \frac{L}{2}], \\ A_3 \sinh(\omega_u(\frac{3L}{2} - x)) + A_4 \sinh(\omega_u(x - \frac{L}{2})), & x \in [\frac{L}{2}, \frac{3L}{2}], \\ A_5 \sinh(\omega_u(2L - x)) + A_6 \sinh(\omega_u(x - \frac{3L}{2})), & x \in [\frac{3L}{2}, 2L], \end{cases}$$

where $\omega_u := \sqrt{\sigma_u/D_u}$. Upon imposing that $u_e(0) = u_e(2L)$, $\partial_x u_e(0) = \partial_x u_e(2L)$, and u_e is continuous at $x = L/2$ and $x = 3L/2$, we obtain that

$$A_1 = A_6 = A_3 + A_4, \quad A_2 = A_3 \frac{\sinh(\omega_u L)}{\sinh(\omega_u L/2)}, \quad A_5 = A_4 \frac{\sinh(\omega_u L)}{\sinh(\omega_u L/2)}.$$

By enforcing the jump conditions for u_e at $x = L/2$ and $x = 3L/2$, we determine A_3 and A_4 as

$$\begin{pmatrix} A_3 \\ A_4 \end{pmatrix} = \frac{\beta_u}{D_u \omega_u (\gamma_u^2 - 4)} \begin{pmatrix} \gamma_u & 2 \\ 2 & \gamma_u \end{pmatrix} \begin{pmatrix} \mu_1^e \\ \mu_2^e \end{pmatrix}, \quad \text{with } \gamma_u := 2 \cosh(\omega_u L) + \frac{\beta_u}{D_u \omega_u} \sinh(\omega_u L).$$

Likewise, we can calculate $v_e(x)$. Then, from the steady-state of the intra-compartment dynamics, we proceed as in §2.1.2 to obtain a non-linear algebraic equation for μ_1^e and μ_2^e characterizing all steady-states of the two-compartment system. We obtain as in §2.1.2 that

$$\begin{pmatrix} f(\mu_1^e, (1, 0)A^{-1}(g_1(\mu_1^e), g_1(\mu_2^e))^T) \\ f(\mu_2^e, (0, 1)A^{-1}(g_1(\mu_1^e), g_1(\mu_2^e))^T) \end{pmatrix} - \frac{\beta_u}{\gamma_u^2 - 4} B \begin{pmatrix} \mu_1^e \\ \mu_2^e \end{pmatrix} = 0, \quad (3.49)$$

where A and B are now defined by

$$A := \frac{\beta_v}{\gamma_v^2 - 4} \tilde{A} + g_2 I, \quad \tilde{A} := \begin{pmatrix} 2\gamma_v \cosh(\omega_v L) - 4 & 4 \cosh(\omega_v L) - 2\gamma_v \\ 4 \cosh(\omega_v L) - 2\gamma_v & 2\gamma_v \cosh(\omega_v L) - 4 \end{pmatrix}, \quad (3.50a)$$

$$B := \begin{pmatrix} 2\gamma_u \cosh(\omega_u L) - 4 & 4 \cosh(\omega_u L) - 2\gamma_u \\ 4 \cosh(\omega_u L) - 2\gamma_u & 2\gamma_u \cosh(\omega_u L) - 4 \end{pmatrix}. \quad (3.50b)$$

Here $\gamma_v := 2 \cosh(\omega_v L) + \frac{\beta_v}{D_v \omega_v} \sinh(\omega_v L)$.

In place of (2.10), the eigenvalues a_1, b_1 and a_2, b_2 of the matrices A and B for the in-phase $q_1 = (1, 1)^T$ and anti-phase $q_2 = (1, -1)^T$ modes are

$$a_1 = \frac{\beta_v}{\gamma_v^2 - 4} [2\gamma_v (\cosh(\omega_v L) - 1) + 4 (\cosh(\omega_v L) - 1)] + g_2 \quad (3.51a)$$

$$a_2 = \frac{\beta_v}{\gamma_v^2 - 4} [2\gamma_v (\cosh(\omega_v L) + 1) - 4 (\cosh(\omega_v L) + 1)] + g_2, \quad (3.51b)$$

$$b_1 = 2\gamma_u (\cosh(\omega_u L) - 1) + 4 (\cosh(\omega_u L) - 1), \quad (3.51c)$$

$$b_2 = 2\gamma_u (\cosh(\omega_u L) + 1) - 4 (\cosh(\omega_u L) + 1). \quad (3.51d)$$

In terms of a_1 and b_1 , and in analogy with (2.11), the symmetric steady-state $(\mu_1^e, \mu_2^e) = \mu_e q_1^T$, is obtained from the scalar algebraic equation

$$f(\mu_e, \frac{g_1(\mu_e)}{a_1}) - \frac{\beta_u}{\gamma_u^2 - 4} b_1 \mu_e = 0. \quad (3.52)$$

As a remark, for the special case where $g = g_1(\mu) - g_2\eta$, we can verify after a direct but tedious calculation that the steady-state condition (3.38) is equivalent to (3.52).

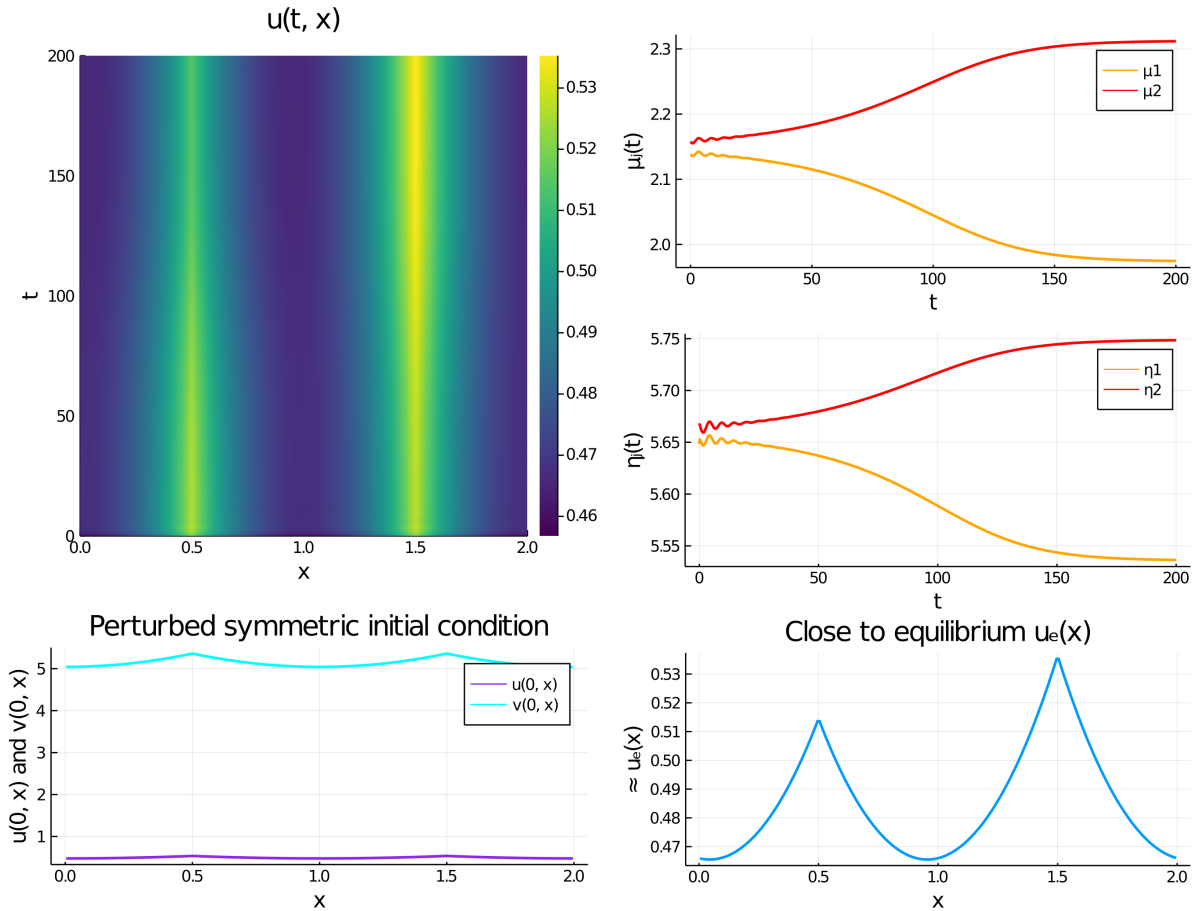


Figure 12: FN kinetics with $n = 2$: For an initial condition near the unstable symmetric branch, and for $z = z_{P,2} \approx 6.63675$ and $\rho = \beta_v/\beta_u = 60$, the full time-dependent solution computed using the BE-RK4 IMEX scheme of Appendix B converges to a stable asymmetric steady-state. For $z = 6.63675$, the pitchfork bifurcation point in ρ is $\rho_p = 50$. Parameters: $D_u = 1, D_v = 2, \sigma_u = \sigma_v = 1, \varepsilon = 0.6, q = 1, L = 1$, and $\beta_u = 0.3$.

3.3 FitzHugh-Nagumo kinetics

To illustrate the theory, we first choose the FN kinetics as given in (2.2). For $n = 2$, for which (3.49), (3.52) and (3.51) apply, the pitchfork points $z_{P,1}$ and $z_{P,2}$ delimiting the pitchfork bubble in z are recovered from the parameter constraint (2.22) in which a_1, a_2, b_1 , and b_2 are now given as in (3.51). For $n = 2$, we can use MatCont [5] on (3.49) to calculate both symmetric and asymmetric steady-states using either z or the binding rate ratio $\rho = \beta_v/\beta_u$ as parameters. The bifurcation diagrams are qualitatively similar to those in Fig. 3 (not shown).

For $n = 2$, in Fig. 12 we show, for an initial condition near the unstable symmetric branch, that the time-dependent numerical solution computed using the BE-RK4 IMEX scheme of Appendix B tends to a stable asymmetric pattern. For $n = 3$, and for a parameter set where the symmetric steady-state is unstable, in Fig. 13 we show the time-dependent convergence to two different stable asymmetric patterns depending on the specific form of the initial perturbation of the symmetric state. For $n = 3$, we conclude from (3.48) and the discussion in §3.1.1 that at the zero-eigenvalue crossing for an asymmetric mode there is a two-dimensional eigenspace for the vector cell perturbation $\phi_{\text{cell},1}$, given by the plane $(1, 1, 1)^T \phi_{\text{cell},1} = 0$.

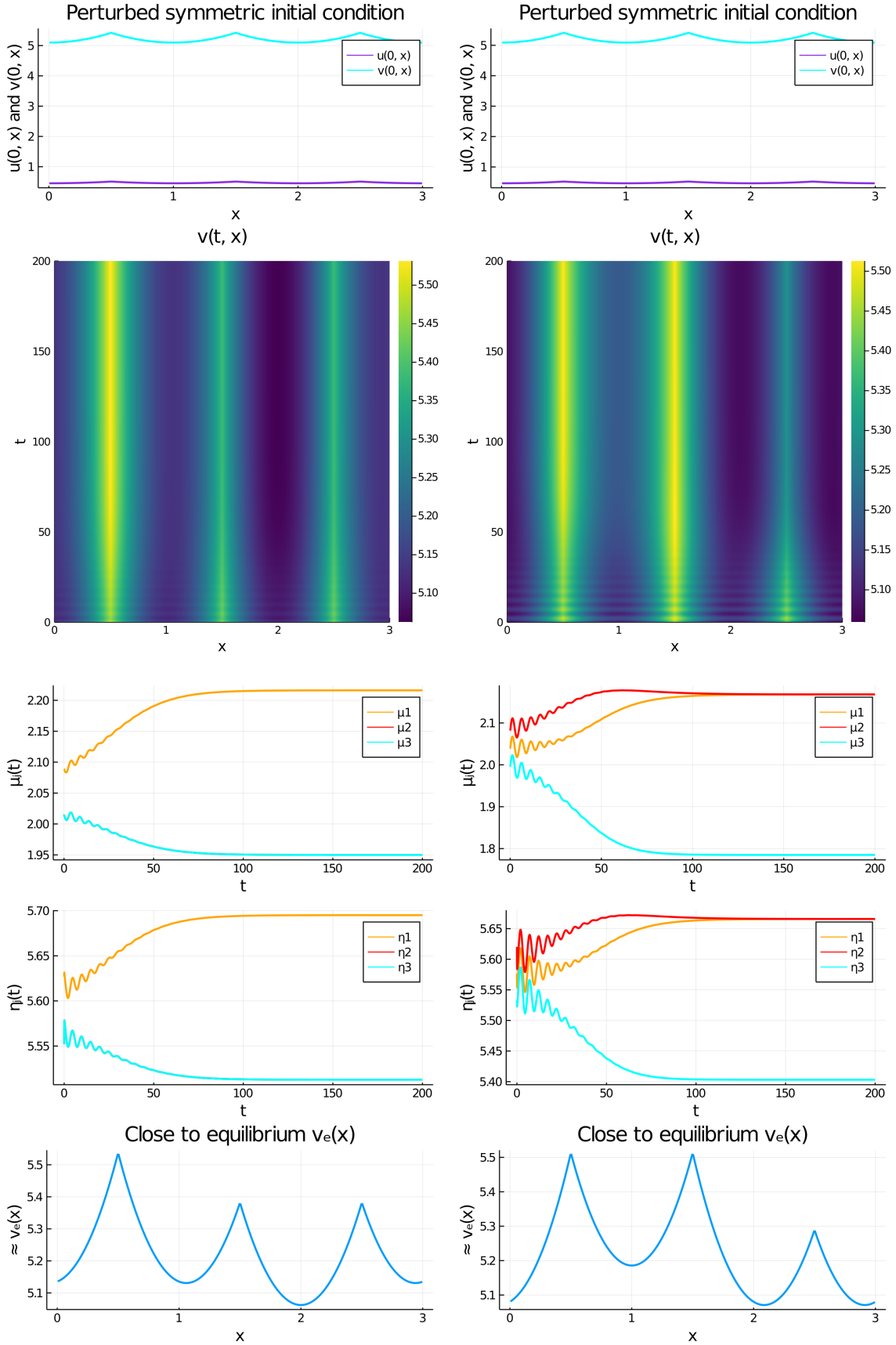


Figure 13: FN kinetics with $n = 3$: Full-numerical time-dependent results from the BE-RK4 IMEX scheme of Appendix B. Left: convergence to a stable asymmetric pattern due to an initial cell perturbation with $\phi_{\text{cell},1} = \mathbf{v}_{c1} = (1, -1/2, -1/2)^T$. Right: convergence to a different stable asymmetric branch due to an initial cell perturbation with $\phi_{\text{cell},1} = (0, \sqrt{3}/2, -\sqrt{3}/2)^T$. Parameters: $D_u = 1, D_v = 2, \sigma_u = \sigma_v = 1, \varepsilon = 0.6, q = 1, L = 1, \beta_u = 0.3, \rho = 120$, and $z = 7$.

3.4 Gierer-Meinhardt kinetics

Next, we consider the periodic problem with GM intra-compartmental kinetics (2.28). By solving (3.49) and (3.52) using MatCont [5], in Fig. 14 we show that the bifurcation diagram of steady-states for $n = 2$ compartments and with $D_u = D_v = 1$ exhibits a hysteresis structure between the symmetric and asymmetric steady-state solution branches.

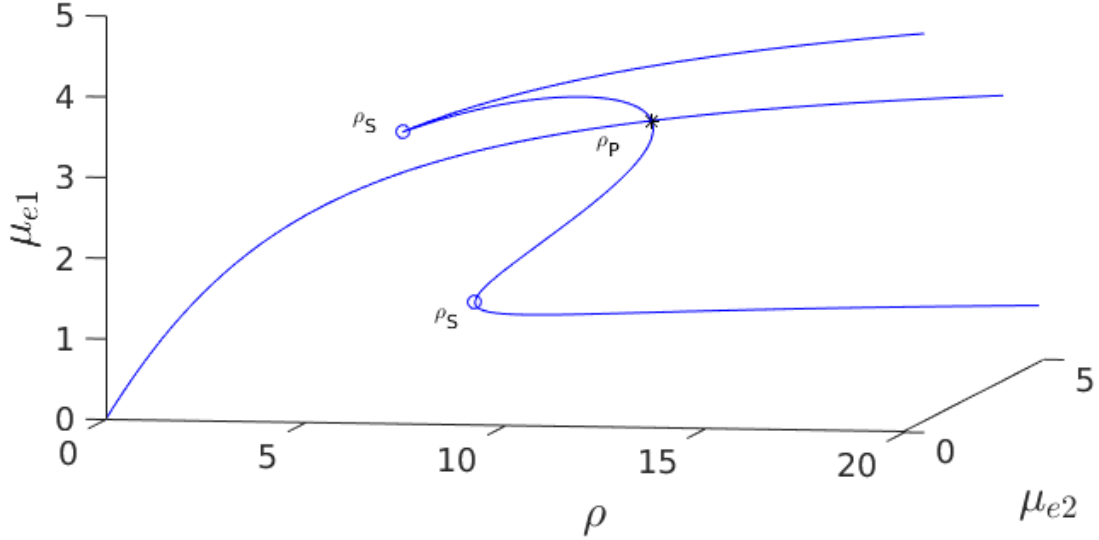


Figure 14: 3-D Bifurcation diagram, exhibiting hysteresis, with bifurcation parameter $\rho = \beta_v/\beta_u$ for steady-states with GM kinetics and $n = 2$ computed from (3.49) using MatCont [5]. The subcritical pitchfork bifurcation point from the symmetric steady-state is at $\rho = \rho_p \approx 11.42015$ and the fold points on the asymmetric branches are at $\rho_f \approx 6.82631$. The symmetric steady-state is linearly stable only for $1 < \rho < \rho_p$, while the asymmetric branches become stable only past the fold points. Parameters: $D_u = D_v = 1, \sigma_u = \sigma_v = 1, L = 1$, and $\beta_u = 0.3$. Note that the geometry of the asymmetric branches near the fold points is just mirrored and it looks different in the figure because of the 3-D plot.

From the numerical results given in Table 3, we observe that asymmetric branches do bifurcate from the symmetric branch even when $D_v/D_u < 1$, and that the range of ρ where hysteresis occurs is larger as the ratio D_v/D_u decreases. In Table 4 we show for $D_u = D_v = 1$ that as β_u is increased beyond $\beta_u = 0.7$ the pitchfork bifurcation switches from sub- to super-critical. The overall trends are qualitatively similar to those given in Tables 1 and 2 for the case of reactive domain boundaries.

Although we have not provided a linear stability theory for the asymmetric steady-state solution branches in Fig. 14, the full PDE numerical results shown in Figs. 15–16, as computed using the BE-RK4 IMEX scheme of Appendix B, confirm the hysteresis structure of Fig. 14 and the prediction of stable asymmetric patterns.

3.5 Rauch-Millonas kinetics

Finally, we briefly show that stable asymmetric patterns can also occur with Rauch-Millonas kinetics (2.32) for $n = 2$ compartments when $D_u = D_v = 1$. Upon solving (3.49) with (2.32) using MatCont [5], in the left and right panels of Fig. 17 we plot bifurcation diagrams of μ_1^e versus either w_v or ρ , respectively. In Fig. 17(left) we observe that asymmetric steady-states occur in a w_v -pitchfork bubble, while from Fig. 17(right) we observe that asymmetric steady-states emerge from a supercritical ρ -pitchfork bifurcation that opens as ρ increases above a threshold. The

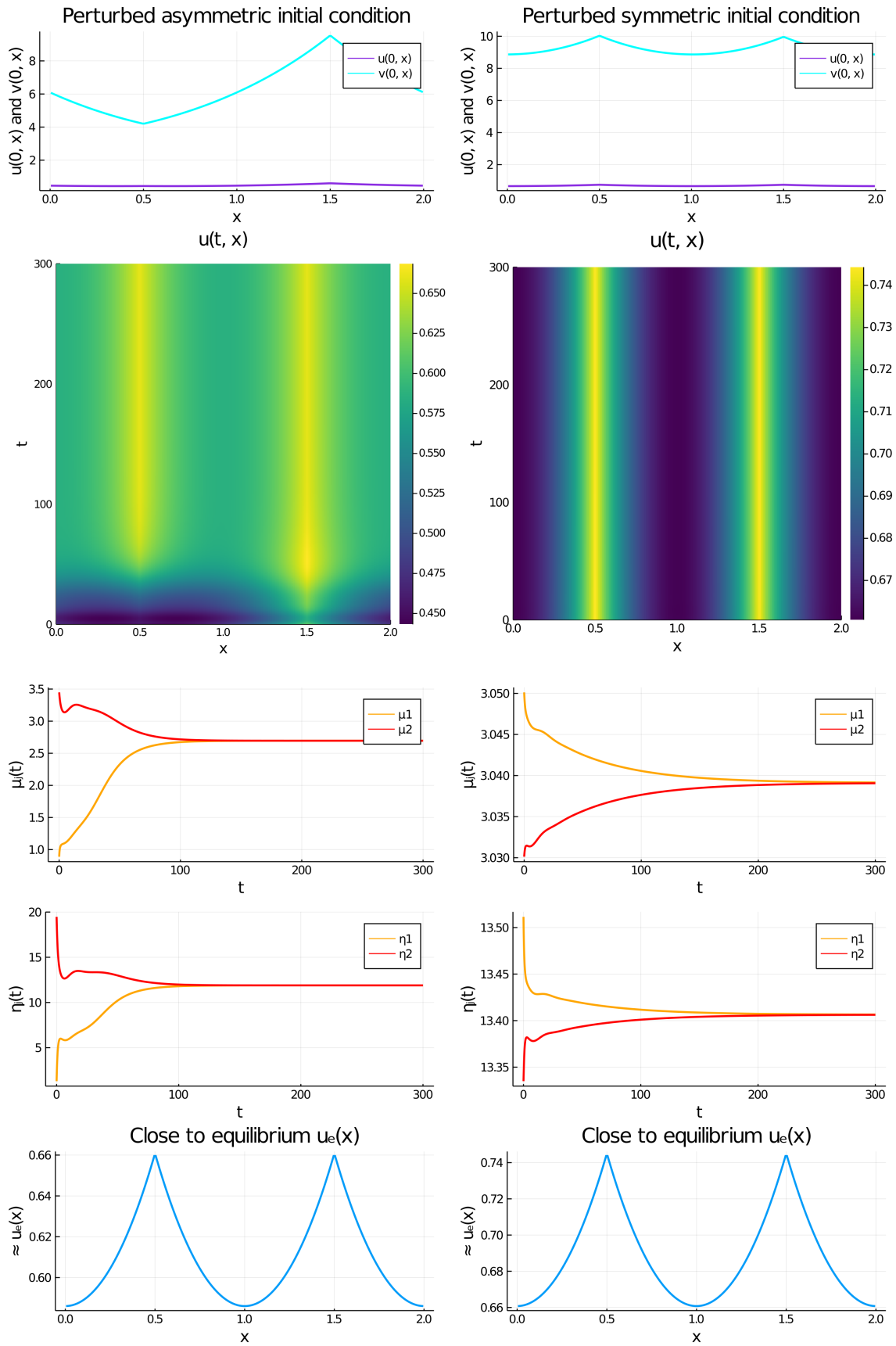


Figure 15: GM kinetics with $n = 2$. Full numerical time-dependent results from the BE-RK4 IMEX scheme. Left: convergence to the stable symmetric branch when $\rho = 6$ starting just prior to the fold point where a stable asymmetric steady-state is born. Right: convergence to the stable symmetric branch for $\rho = 9$ with an initial condition near the symmetric branch. Remaining parameter values are as in the caption to Fig. 14.

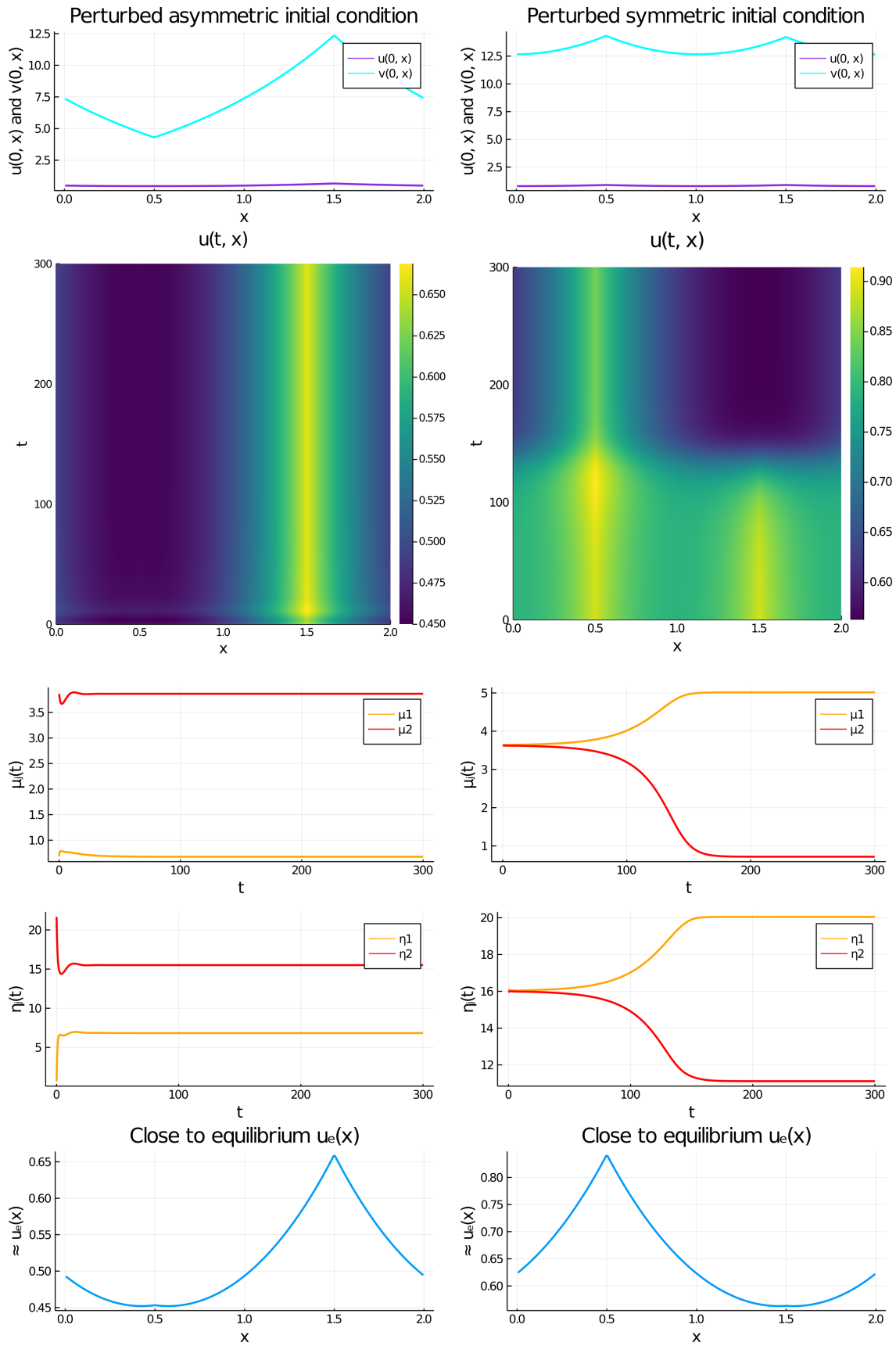


Figure 16: GM kinetics with $n = 2$. Full numerical time-dependent results from the BE-RK4 IMEX scheme. Left: convergence to a stable asymmetric branch when $\rho = 9$ starting close to the stable asymmetric branch. Right: convergence to a stable asymmetric branch when $\rho = 25$ starting close to the unstable symmetric branch. Remaining parameter values are as in the caption to Fig. 14.

$\frac{D_v}{D_u}$	0.4	0.5	0.6	0.7	0.8	0.9	1
ρ_p	> 100	53.17080	35.32088	28.23715	24.43531	22.06333	20.44213
μ_e		8.21230	7.81358	7.53645	7.33272	7.17669	7.05336
ρ_f		6.25939	5.66710	5.29081	5.03058	4.83989	4.69415
μ_1^e		4.45524	4.23893	4.08858	3.97806	3.89341	3.82650
μ_2^e		0.37314	0.35503	0.34243	0.33318	0.32609	0.32048
$\frac{D_v}{D_u}$	1.1	1.2	1.3	1.4	1.5	1.6	
ρ_p	19.26390	18.36889	17.66592	17.09916	16.63252	...	
μ_e	6.95344	6.87085	6.80144	6.74229	6.69129		
ρ_f	4.57915	4.48608	4.40922	4.34468	4.28971		
μ_1^e	3.77230	3.72749	3.68983	3.65775	3.63008		
μ_2^e	0.31594	0.31219	0.30904	0.30635	0.30403		

Table 3: Numerical values (rounded to 5th decimal place) of the subcritical pitchfork bifurcation point ρ_p for the symmetric branch and the fold points ρ_f along the asymmetric branches. Bifurcation values for the symmetric (μ_e) and one of the asymmetric (μ_1^e , μ_2^e) solution branches are listed. As D_v/D_u decreases, the range of ρ where hysteresis occurs increases. Parameters: $D_u = 1$, $\sigma_u = \sigma_v = 1$, $L = 1$, and $\beta_u = 0.1$.

full-numerical simulations shown in Fig. 18 for $\rho = 15$ and $w_v = w_v^{P,2}$ are consistent with the prediction of Fig. 17(right) of stable asymmetric patterns.

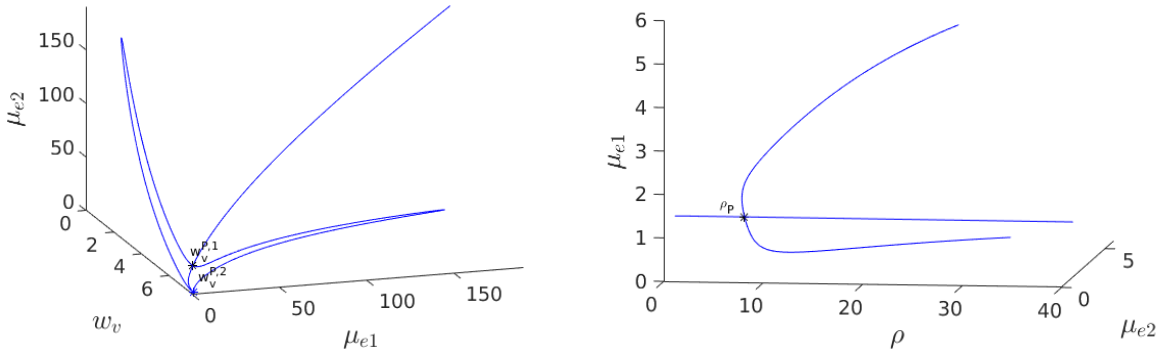


Figure 17: 3-D Bifurcation diagrams for Rauch-Millonas kinetics (2.32) with $n = 2$ computed from (3.49) using MatCont [5]. Left: Plot of μ_1^e showing that asymmetric steady-states occur inside a degenerate pitchfork bubble bounded by $w_v^{P,1} \approx 6.34518$ and $w_v^{P,2} \approx 7.64062$ when $\rho = \beta_v/\beta_u = 7$. Right: Supercritical pitchfork bifurcation in ρ from the symmetric branch occurs when $w_v = w_v^{P,2}$. Stable asymmetric branches occur past this threshold in ρ . Parameters: $D_u = D_v = 1$, $\sigma_u = \sigma_v = 0.01$, $c_u = c_v = 1$, $q_u = 1/100$, $q_v = 7$, $\alpha_1^u = 600$, $\alpha_2^u = 6$, $\gamma_1^u = 100$, $\gamma_2^u = 1/10$, and $\beta_u = 0.3$.

4 Discussion

We have formulated and analyzed a new class of 1-D compartmental-reaction diffusion system in which a two-component nonlinear reaction kinetics is restricted to the domain boundaries and where two bulk diffusing species effectively couple the spatially localized reactions. For the case of a common reaction kinetics, and when one of the kinetic species has a linear dependence, we have derived a nonlinear algebraic system characterizing the steady-states of the model. Through a bifurcation analysis and from path-following numerical methods we have shown that symmetry-

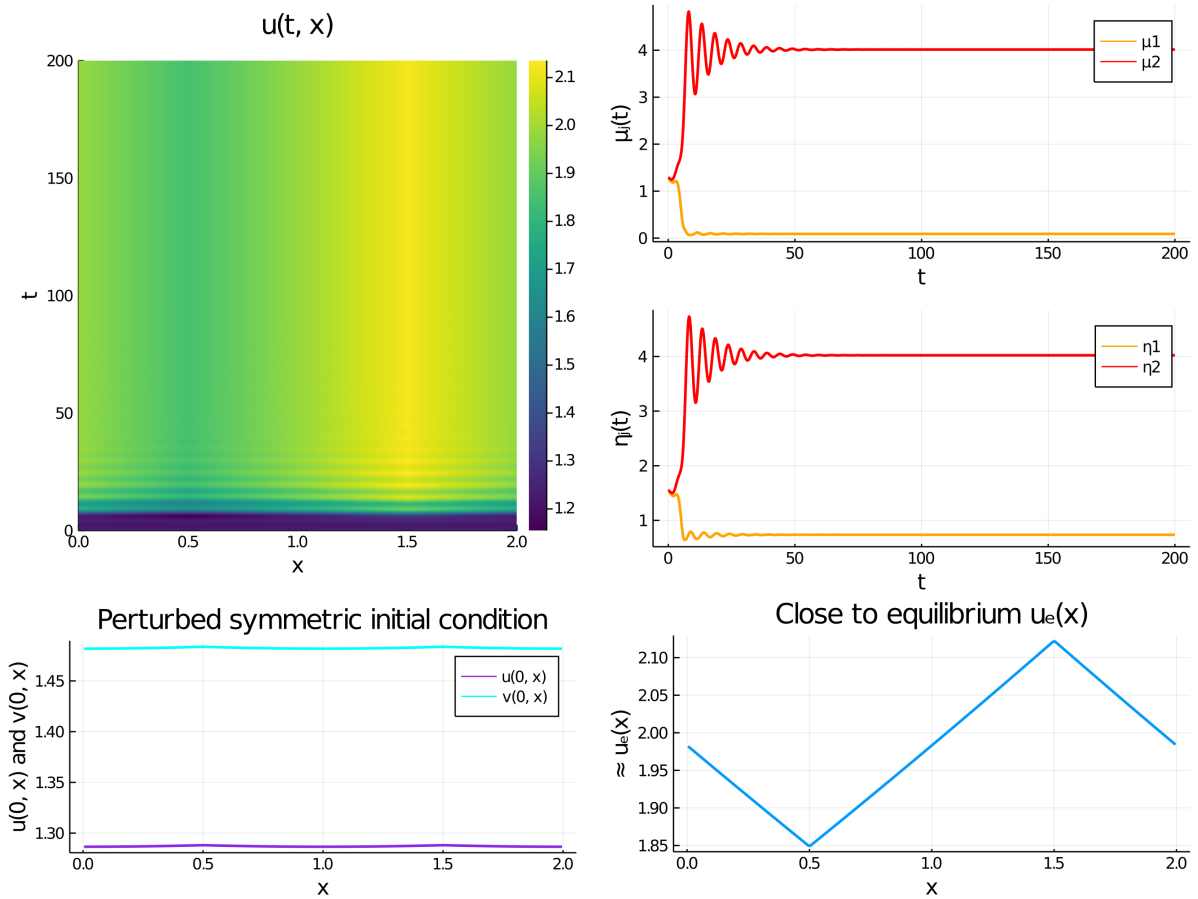


Figure 18: Raich-Millonas kinetics with $n = 2$. For an initial condition near the unstable symmetric branch, and for $\rho = 15$ and $w_v = w_v^{P,2}$, the full time-dependent solution computed using the BE-RK4-IMEX scheme of Appendix B converges to a stable asymmetric steady-state. The results are consistent with the prediction from the bifurcation diagram in Fig. 17(right). The remaining parameter values are as in the caption of Fig. 17. Observe that u_e is nearly piecewise linear owing to the fact that the bulk degradation σ_u is very small, i.e. $\sigma_u = 0.01$.

β_u	0.05	0.1	0.15	0.2	0.25	0.3	0.35	0.4
ρ_p	36.28648	20.44213	15.39744	13.09728	11.94362	11.42015	11.32738	11.59667
μ_e	12.90881	7.05336	5.11479	4.15511	3.58673	3.21380	2.95240	2.76056
ρ_f	4.32660	4.69415	5.11246	5.59447	6.15768	6.82631	7.63502	8.63523
μ_1^e	3.91408	3.82650	3.73728	3.64635	3.55352	3.45845	3.36053	3.25882
μ_2^e	0.16492	0.32048	0.46828	0.60972	0.74617	0.87895	1.00951	1.13950
β_u	0.45	0.5	0.55	0.6	0.65	0.7		
ρ_p	12.23745	13.33412	15.08439	17.91935	22.88248	33.18867		
μ_e	2.61497	2.50167	2.41175	2.33930	2.28021	2.231556		
ρ_f	9.90668	11.58010	13.88586	17.27125	22.73469	-		
μ_1^e	3.15185	3.03717	2.91034	2.76171	2.55994	-		
μ_2^e	1.27099	1.40694	1.55225	1.71692	1.93262	-		

Table 4: Similar caption as in Table 3 except that the bifurcation quantities for $\rho = \beta_v/\beta_u$ are tabulated for various values of β_u when $D_v = D_u = 1$. The range where hysteresis occurs decreases as β_u increases, and when $\beta_u \approx 0.7$ the pitchfork bifurcation switches from sub- to super critical. Other parameters are as in the caption of Table 3.

breaking pitchfork bifurcations can occur even when the two bulk diffusing species have identical or very comparable diffusivities. The linear stability properties of the symmetric steady-state was investigated numerically by deriving a nonlinear matrix eigenvalue problem characterizing both in-phase and anti-phase perturbations of a symmetric steady-state. Through numerical computations of branches of steady-state solutions together with the numerical solution of the nonlinear matrix eigenvalue problem, the theory was illustrated for either FitzHugh-Nagumo, Gierer-Meinhardt, or Rauch-Millonas reaction kinetics. The theoretical prediction of symmetry-breaking leading to stable asymmetric patterns in these models was confirmed through full time-dependent PDE computations. Overall, it was shown that it is the ratio of the two binding rates to the compartments that controls whether stable asymmetric patterns can occur. This is in contrast to the case of a traditional activator-inhibitor RD system where stable spatial patterns exist only for a sufficiently large, but typically biologically unrealistic, diffusivity ratio of the two diffusing species. For FitzHugh-Nagumo and Rauch-Millonas kinetics we have also shown that stable asymmetric patterns can emerge from a symmetric pattern at a fixed binding rate ratio when a control parameter in the intracellular kinetics is varied. Extensions of the analytical theory to treat a periodic chain of reaction compartments was made, and the results confirmed through full PDE simulations.

We remark that our findings are qualitatively similar to those associated with a postulated diffusive transport mechanism for biological morphogens, referred to as a **binding-mediated hindrance diffusion process** [35], in which a differential binding rate ratio on the cell boundaries for two morphogen species with comparable diffusivities was suggested to provide the large **effective** diffusivity ratio that is required for pattern formation and symmetry-breaking in tissues. However, since our condition (2.16) for the existence of symmetry-breaking bifurcations is highly implicit in the bulk diffusivities, it seems rather intractable analytically to isolate via a simple scaling analysis an **effective diffusivity** bifurcation parameter for the bulk species that incorporates the membrane binding rate ratio and/or the ratio of bulk degradation rates. An effective diffusivity ratio condition was also derived analytically in [26] for a $2 + 1$ RD system with an immobile substrate. It is an open problem to isolate an effective diffusivity ratio parameter for our compartmental-reaction diffusion system that encapsulates analytically how the symmetry-breaking bifurcation point depends on the membrane binding rate ratio and the ratio of bulk degradation rates.

In the context of our 1-D framework, there are four main additional open problems. Firstly, it would be worthwhile to formulate a linear stability problem for asymmetric patterns of the

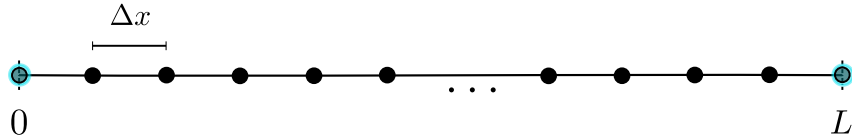
1-D compartmental-reaction diffusion system, while allowing for arbitrary reaction kinetics. Secondly, it would be interesting to extend the weakly nonlinear analysis of [37], which dealt with one-bulk diffusing species, to our compartmental-reaction diffusion setting. With this extension, amplitude equations near the symmetry-breaking bifurcation would be valuable so as to classify whether the bifurcation is sub- or super-critical, and thereby predict whether the emerging asymmetric patterns are linearly stable or unstable. Finally, it would be interesting to analytically represent the time-dependent bulk diffusion fields in terms of a time-dependent Green function so as to reduce the bulk-cell system to an integro-differential system of ODEs with memory. In this setting, large amplitude solutions, including time-periodic solutions, would represent a new frontier to be investigated. A further extension of our 1-D model would be to investigate how the symmetry-breaking bifurcations are influenced by random noise arising from the compartmental reaction kinetics. In [19] it was shown that including stochasticity in RD systems can lower the threshold for the onset of pattern formation (see [10] for an overview of stochastic modeling in RD systems).

An important open direction is to analyze symmetry-breaking behavior associated with a similar modeling framework in a 2-D spatial setting where intra-compartmental reactions occur only within a disjoint collection of small circular disks within a bounded 2-D domain. In this context, two bulk diffusing species with comparable diffusivities can effectively be transported across the compartment boundaries as regulated by certain binding rates. This exchange between the compartments and the bulk medium can either trigger or modulate the intra-compartmental reactions. Similar bulk-cell models in 2-D, but with only one diffusing bulk species, have been analyzed recently to model quorum-sensing behavior (cf. [17], [22], [45], [13]).

Another possible extension of our modeling framework is to consider a compartmental-reaction diffusion system on a network. In this graph-theoretic setting, the reaction kinetics are restricted to the nodes of the graph, while two bulk species are taken to diffuse along the edges. Related network models of this type have been analyzed in [34], [7] and [28] for general multi-component systems, and in [2] for a spatially-extended SIR epidemic model.

A CN-RK4 IMEX method on a non-centered grid

In this appendix we provide details on the numerical method used to solve the 2-cell system of §2. For illustration, we focus on the FN kinetics as in §2.2. Let $M \in \mathbb{N} \setminus \{0, 1\}$, $N \in \mathbb{N} \setminus \{0, 1\}$, and let $\Delta x := \frac{L}{N-1}$ and $\Delta t := \frac{t_f}{M-1}$ be, respectively, the spatial step and the time step for some final time t_f . Let then $\{x_n\}_n$ with $x_n := (n-1)\Delta x$, $n \in \{1, \dots, N\}$, be the spatial grid and $\{t_m\}_m$ with $t_m := (m-1)\Delta t$, $m \in \{1, \dots, M\}$, be the temporal grid.



We discretize the 1-D Laplacian by the centered scheme

$$\partial_{xx}u(t, x_n) = \frac{u(t, x_{n+1}) - 2u(t, x_n) + u(t, x_{n-1}))}{(\Delta x)^2} + \mathcal{O}(\Delta x^2),$$

for all points away from the boundary, i.e., for $n \in \{2, 3, \dots, N-1\}$. For $n = 1$, use the Robin boundary conditions of our system, so that

$$\partial_{xx}u(t, 0) = \frac{\frac{u(t, \Delta x) - u(t, 0)}{\Delta x} - \partial_x u(t, 0)}{\frac{1}{2}\Delta x} + \mathcal{O}(\Delta x) = \frac{u(t, \Delta x) - u(t, 0)}{\frac{1}{2}(\Delta x)^2} - \frac{\beta_u}{D_u} \frac{u(t, 0) - \mu_1(t)}{\frac{1}{2}\Delta x} + \mathcal{O}(\Delta x).$$

Similarly, for $x = L$, we have

$$\partial_{xx}u(t, L) = \frac{\partial_x u(t, L) - \frac{u(t, L) - u(t, L - \Delta x)}{\Delta x}}{\frac{1}{2}\Delta x} + \mathcal{O}(\Delta x) = \frac{\beta_u}{D_u} \frac{\mu_2(t) - u(L, t)}{\frac{1}{2}\Delta x} - \frac{u(t, L) - u(t, L - \Delta x)}{\frac{1}{2}(\Delta x)^2} + \mathcal{O}(\Delta x).$$

This yields the discretization matrix defined by

$$L_{\Delta x}^u := \begin{pmatrix} -2 - 2\frac{\beta_u}{D_u}\Delta x & 2 & 0 & \dots & & 0 \\ 1 & -2 & 1 & 0 & \dots & 0 \\ & & \ddots & \ddots & \ddots & \\ & & & 1 & -2 & 1 \\ & & & & \ddots & \ddots & \ddots \\ 0 & \dots & 0 & 2 & -2 - \frac{\beta_u}{D_u}\Delta x & \dots \end{pmatrix},$$

so that to $\mathcal{O}(\Delta x)$ we have

$$\frac{d}{dt} \begin{pmatrix} u(t, x_1) \\ u(t, x_2) \\ \vdots \\ u(t, x_{N-1}) \\ u(t, x_N) \end{pmatrix} = \frac{D_u}{(\Delta x)^2} L_{\Delta x}^u \begin{pmatrix} u(t, x_1) \\ u(t, x_2) \\ \vdots \\ u(t, x_{N-1}) \\ u(t, x_N) \end{pmatrix} + \frac{1}{\Delta x} \begin{pmatrix} 2\beta_u\mu_1(t) \\ 0 \\ \vdots \\ 0 \\ 2\beta_u\mu_2(t) \end{pmatrix} - \sigma_u \begin{pmatrix} u(t, x_1) \\ u(t, x_2) \\ \vdots \\ u(t, x_{N-1}) \\ u(t, x_N) \end{pmatrix}.$$

The discretization matrix $L_{\Delta x}^v$ can be obtained analogously from the equations for v .

Then, upon including the intracellular FN kinetics of (2.2), we obtain the lumped system

$$\frac{d}{dt} w = \mathcal{L}w + \mathcal{N}[w] + \vartheta, \quad (\text{A.53})$$

where

$$w := \begin{pmatrix} u(t, x_1) \\ \vdots \\ u(t, x_N) \\ v(t, x_1) \\ \vdots \\ v(t, x_N) \\ \mu_1(t) \\ \eta_1(t) \\ \mu_2(t) \\ \eta_2(t) \end{pmatrix}, \quad \mathcal{N}[w] := \begin{pmatrix} 0 \\ \vdots \\ 0 \\ 0 \\ \vdots \\ 0 \\ -q(\mu_1 - 2)^3 \\ 0 \\ -q(\mu_2 - 2)^3 \\ 0 \end{pmatrix}, \quad \vartheta := \begin{pmatrix} 0 \\ \vdots \\ 0 \\ 0 \\ \vdots \\ 0 \\ 4 \\ 0 \\ 4 \\ 0 \end{pmatrix},$$

and where the linear matrix operator \mathcal{L} is defined as

$$\mathcal{L} := \begin{pmatrix} & & & 2\frac{\beta_u}{\Delta x} & 0 & 0 & 0 \\ & \frac{D_u}{(\Delta x)^2} L_{\Delta x}^u - \sigma_u I & & \vdots & & \vdots & \\ & & & 0 & 0 & 2\frac{\beta_u}{\Delta x} & 0 \\ & & & 0 & 2\frac{\beta_v}{\Delta x} & 0 & 0 \\ & & \frac{D_v}{(\Delta x)^2} L_{\Delta x}^v - \sigma_v I & \vdots & & \vdots & \\ \beta_u & & & 0 & 0 & 0 & 2\frac{\beta_v}{\Delta x} \\ 0 & 0 & 0 & 0 & 1 - \beta_u & -1 & 0 \\ 0 & 0 & \beta_v & 0 & \varepsilon z & -\varepsilon - \beta_v & 0 \\ 0 & \beta_u & 0 & 0 & 0 & 0 & 1 - \beta_u \\ 0 & 0 & 0 & \beta_v & 0 & 0 & \varepsilon z & -\varepsilon - \beta_v \end{pmatrix}.$$

As inspired by the operator-splitting approach of [3], we consider the split equations

$$\frac{d}{dt} w_L = \mathcal{L}w + \vartheta, \quad \frac{d}{dt} w_N = \mathcal{N}[w],$$

for a *single* time step of length Δt , and note that $w(t) = w_L(t) + w_N(t)$. The affine equation can easily be integrated implicitly with the Crank-Nicholson scheme (CN) yielding an $\mathcal{O}(\Delta t^2)$ -error and the nonlinear equation can be approximated with the classical Runge-Kutta scheme (RK4) yielding an $\mathcal{O}(\Delta t^5)$ error. All combined, this gives the scheme for the full numerical solution at time step $m + 1$. Denoting the numerical solution at time step t_m by w_m , we have

$$\begin{aligned} \frac{w_{m+1} - w_m}{\Delta t} &= \frac{1}{2}(\mathcal{L}w_{m+1} + \mathcal{L}w_m) + \frac{1}{6}(k_{1,m} + 2k_{2,m} + 2k_{3,m} + k_{4,m}) + \vartheta \\ \Leftrightarrow w_{m+1} &= (I - \frac{\Delta t}{2}\mathcal{L})^{-1}((I + \frac{\Delta t}{2}\mathcal{L})w_m + \frac{\Delta t}{6}(k_{1,m} + 2k_{2,m} + 2k_{3,m} + k_{4,m}) + \Delta t\vartheta) \end{aligned}$$

where the weights for RK4 are given by $k_{1,m} := \mathcal{N}[w_m]$, $k_{2,m} := \mathcal{N}[w_m + \frac{\Delta t}{2}k_{1,m}]$, $k_{3,m} := \mathcal{N}[w_m + \frac{\Delta t}{2}k_{2,m}]$, and $k_{4,m} := \mathcal{N}[w_m + \Delta t k_{3,m}]$.

B BE-RK4 IMEX method on a centered grid

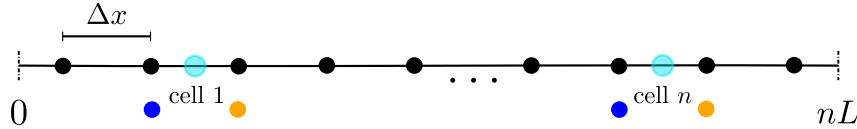
In this appendix we provide details on the numerical method used to solve the ring-cell system of §3. For illustration, we again use the FN kinetics (2.2) as in §3.3.

Let $N \in \mathbb{N} \setminus \{0, 1\}$ be even and denote the number of grid points per fundamental domain with centered cell. Let $M \in \mathbb{N} \setminus \{0, 1\}$ and label $\Delta x := \frac{L}{N}$ and $\Delta t := \frac{t_f}{M-1}$, respectively, as the spatial step and the time step for some final time t_f . We let $\{x_k\}_k$ with $x_k := (k-1)\Delta x$, $k \in \{1, \dots, N\}$, be the spatial grid while $\{t_m\}_m$ with $t_m := (m-1)\Delta t$, $m \in \{1, \dots, M\}$ is the temporal grid. We note that $x_{nN} = nL - \frac{\Delta x}{2}$ and that the j -th cell is centered exactly in between $x_{\frac{2j-1}{2}N}$ and $x_{\frac{2j-1}{2}N+1}$ for $j \in \{1, \dots, n\}$.

We discretize the 1-D Laplacian by the centered scheme

$$\Delta u(t, x_k) = \frac{u(t, x_{k+1}) - 2u(t, x_k) + u(t, x_{k-1}))}{(\Delta x)^2} + \mathcal{O}(\Delta x^2),$$

for all points away from the cells, i.e., for $k \in \{1, \dots, nN\} \setminus \cup\{\frac{2j-1}{2}N, \frac{2j-1}{2}N + 1\}$.



For $k_j := \frac{2j-1}{2}N$, which labels the index of the grid point to the left of the j -th cell, we discretize the 1-D Laplacian by

$$\begin{aligned} \partial_{xx}u(t, x_{k_j}) &= \frac{\tilde{u}_{k_j+1}(t) - 2u(t, x_{k_j}) + u(t, x_{k_j-1}))}{(\Delta x)^2} + \mathcal{O}((\Delta x)^2), \\ \partial_{xx}u(t, x_{k_j+1}) &= \frac{u(t, x_{k_j+2}) - 2u(t, x_{k_j+1}) + \tilde{u}_{k_j}(t)}{(\Delta x)^2} + \mathcal{O}((\Delta x)^2), \end{aligned}$$

where the coloured points are values at the ghost points depicted in the schematic figure above and are obtained from

$$\begin{aligned} \frac{u(t, x_{k_j+1}) + \tilde{u}_{k_j}(t)}{2} &= \frac{\tilde{u}_{k_j+1}(t) + u(t, x_{k_j})}{2}, \quad (\text{continuity condition}) \\ \frac{u(t, x_{k_j+1}) - \tilde{u}_{k_j}(t)}{\Delta x} - \frac{\tilde{u}_{k_j+1}(t) - u(t, x_{k_j})}{\Delta x} &= \frac{\beta_u}{D_u} \left(\frac{u(t, x_{k_j+1}) + u(t, x_{k_j})}{2} - \mu_j(t) \right), \quad (\text{jump condition}). \end{aligned}$$

Upon solving for the ghost point values we get

$$\begin{aligned} \tilde{u}_{k_j}(t) &= \frac{1}{2} \left(2 - \frac{\beta_u \Delta x}{2D_u} \right) u(t, x_{k_j}) + \frac{\beta_u \Delta x}{2D_u} \mu_j(t) - \frac{\beta_u \Delta x}{4D_u} u(t, x_{k_j+1}), \\ \tilde{u}_{k_j+1}(t) &= -\frac{\beta_u \Delta x}{4D_u} u(t, x_{k_j}) + \frac{\beta_u \Delta x}{2D_u} \mu_j(t) + \frac{1}{2} \left(2 - \frac{\beta_u \Delta x}{2D_u} \right) u(t, x_{k_j+1}). \end{aligned}$$

This yields the discretization matrix defined by

$$L_{\Delta x}^u := \begin{pmatrix} -2 & 1 & 0 & \dots & 0 & 1 \\ 1 & -2 & 1 & 0 & \dots & 0 \\ & & \ddots & & & \\ & & & 1 & -2 - \frac{\beta_u \Delta x}{4D_u} & 1 - \frac{\beta_u \Delta x}{4D_u} \\ & & & 1 - \frac{\beta_u \Delta x}{4D_u} & -2 - \frac{\beta_u \Delta x}{4D_u} & 1 \\ & & & & & \ddots \\ 1 & 0 & \dots & & 0 & -2 & 1 \end{pmatrix}$$

satisfying, to $\mathcal{O}(\Delta x)$,

$$\frac{d}{dt} \begin{pmatrix} u(t, x_1) \\ u(t, x_2) \\ \vdots \\ u(t, x_{k_j}) \\ u(t, x_{k_j+1}) \\ \vdots \\ u(t, x_{N-1}) \\ u(t, x_N) \end{pmatrix} = \frac{D_u}{(\Delta x)^2} L_{\Delta x}^u \begin{pmatrix} u(t, x_1) \\ u(t, x_2) \\ \vdots \\ u(t, x_{k_j}) \\ u(t, x_{k_j+1}) \\ \vdots \\ u(t, x_{N-1}) \\ u(t, x_N) \end{pmatrix} + \frac{1}{\Delta x} \begin{pmatrix} 0 \\ \vdots \\ 0 \\ \frac{\beta_u}{2} \mu_j(t) \\ \frac{\beta_u}{2} \mu_j(t) \\ 0 \end{pmatrix} - \sigma_u \begin{pmatrix} u(t, x_1) \\ u(t, x_2) \\ \vdots \\ u(t, x_{k_j}) \\ u(t, x_{k_j+1}) \\ \vdots \\ u(t, x_{N-1}) \\ u(t, x_N) \end{pmatrix}.$$

Note the abuse of notation for the entries indexed by j . Read here that such entries are in $L_{\Delta x}^u$ for each $j \in \{1, \dots, n\}$. The discretization matrix $L_{\Delta x}^v$ can be obtained analogously from the equations for v .

Next, the intracellular FN reaction kinetics (2.2) are approximated by

$$\begin{aligned} \frac{d}{dt} \mu_j(t) &= (1 - \beta_u) \mu_j(t) - q(\mu_j(t) - 2)^3 + 4 - \eta_j(t) + \beta_u \left(\frac{u(t, x_{k_j}) + u(t, x_{k_j+1})}{2} \right), \\ \frac{d}{dt} \eta_j(t) &= \varepsilon z \mu_j(t) + (-\varepsilon - \beta_v) \eta_j(t) + \beta_v \left(\frac{v(t, x_{k_j}) + v(t, x_{k_j+1})}{2} \right). \end{aligned}$$

Then, upon including the intracellular FN kinetics, we obtain the lumped system

$$\frac{d}{dt} w = \mathcal{L}w + \mathcal{N}[w] + \vartheta, \quad (\text{B.54})$$

where now we define

$$w := \begin{pmatrix} u(t, x_1) \\ \vdots \\ u(t, x_{k_j}) \\ u(t, x_{k_j+1}) \\ \vdots \\ u(t, x_N) \\ v(t, x_1) \\ \vdots \\ v(t, x_{k_j}) \\ v(t, x_{k_j+1}) \\ \vdots \\ v(t, x_N) \\ \mu_j(t) \\ \eta_j(t) \end{pmatrix}, \quad \mathcal{N}[w] := \begin{pmatrix} 0 \\ \vdots \\ 0 \\ 0 \\ \vdots \\ 0 \\ 0 \\ \vdots \\ 0 \\ 0 \\ \vdots \\ 0 \\ -q(\mu_j - 2)^3 \\ 0 \end{pmatrix}, \quad \vartheta := \begin{pmatrix} 0 \\ \vdots \\ 0 \\ 0 \\ \vdots \\ 0 \\ 0 \\ \vdots \\ 0 \\ 0 \\ \vdots \\ 0 \\ 4 \\ 0 \end{pmatrix},$$

and where the linear matrix operator \mathcal{L} is now defined by

$$\mathcal{L} := \begin{pmatrix} & & & & & & & & 0 & 0 \\ & & & & & & & & \vdots & \\ & & & & & & & & \frac{\beta_u}{2\Delta x} & 0 \\ & & & & & & & & \frac{\beta_u}{2\Delta x} & 0 \\ & & & & & & & & \vdots & \\ & & & & & & & & 0 & 0 \\ & & & & & & & & 0 & 0 \\ & & & & & & & & \vdots & \\ & & & & & & & & 0 & 0 \\ & & & & & & & & \frac{\beta_v}{2\Delta x} & \\ & & & & & & & & \frac{\beta_v}{2\Delta x} & \\ & & & & & & & & \vdots & \\ & & & & & & & & 0 & 0 \\ 0 & & & & & & & & 0 & 1 - \beta_u & -1 \\ 0 & & & & & & & & \frac{\beta_u}{2} & \frac{\beta_u}{2} & 0 & 0 & 0 & 0 & \frac{\beta_v}{2} & \frac{\beta_v}{2} & 0 & \varepsilon z & -\varepsilon - \beta_v \end{pmatrix}.$$

Again note that there is an abuse of notation for the j -indexed rows, including the reaction kinetics rows, as it refers to all $j \in \{1, \dots, n\}$.

With the operator-splitting approach inspired by [3], we again consider the split equations

$$\frac{d}{dt}w_L = \mathcal{L}w + \vartheta, \quad \frac{d}{dt}w_N = \mathcal{N}[w]$$

for a *single* time step of length Δt , and note that $w(t) = w_L(t) + w_N(t)$. The affine equation is approximated implicitly with the Backward-Euler scheme (BE) yielding an $\mathcal{O}(\Delta t)$ -error, while the nonlinear equation is integrated explicitly using the classical Runge-Kutta scheme (RK4) yielding an $\mathcal{O}(\Delta t^5)$ error. All combined, this gives the scheme for the full numerical solution at time step $m + 1$. Denoting the numerical solution at time step t_m by w_m , we have

$$\begin{aligned} \frac{w_{m+1} - w_m}{\Delta t} &= \mathcal{L}w_{m+1} + \frac{1}{6}(k_{1,m} + 2k_{2,m} + 2k_{3,m} + k_{4,m}) + \vartheta \\ \Leftrightarrow w_{m+1} &= (I - \Delta t \mathcal{L})^{-1} \left(w_m + \frac{\Delta t}{6}(k_{1,m} + 2k_{2,m} + 2k_{3,m} + k_{4,m}) + \Delta t \vartheta \right), \end{aligned}$$

where the weights for RK4 are given by $k_{1,m} := \mathcal{N}[w_m]$, $k_{2,m} := \mathcal{N}[w_m + \frac{\Delta t}{2}k_{1,m}]$, $k_{3,m} := \mathcal{N}[w_m + \frac{\Delta t}{2}k_{2,m}]$, and $k_{4,m} := \mathcal{N}[w_m + \Delta t k_{3,m}]$.

We remark that this scheme is of order $\mathcal{O}((\Delta x)^2)$ in contrast to the order $\mathcal{O}(\Delta x)$ scheme of Appendix A. This is due to using a centered grid with two ghost points per cell. Also note that we have used the implicit $\mathcal{O}(\Delta t)$ -scheme BE instead of the implicit $\mathcal{O}((\Delta t)^2)$ -scheme CN since the latter can possibly generate numerical instabilities. As a result, the scheme presented in this appendix is more somewhat robust than that given in Appendix A.

Authors' Contributions: The authors contributed equally to this article.

Competing Interests: There are no competing interests.

Funding: Merlin Pelz was supported by a Four-Year-Graduate-Fellowship from UBC. M. J. Ward was supported by the NSERC Discovery Grant Program.

Acknowledgements: The authors are thankful to Prof. Brian Wetton for his help with introducing ghost points for the BE-RK4 IMEX numerical scheme.

References

- [1] R. E. Baker, E. A. Gaffney, and P. K. Maini. Partial differential equations for self-organization in cellular and developmental biology. *Nonlinearity*, 21(11):R251, 2008.
- [2] C. Besse and G. Faye. Dynamics of epidemic spreading on graphs. *J. Math. Bio.*, 82(6):1–52, 2021.
- [3] M. Cross and H. Greenside. *Pattern formation and dynamics in nonequilibrium systems*. Cambridge University Press, 2009.
- [4] D. Cusseddu, L. Edelstein-Keshet, J. A. Mackenzie, S. Portet, and A. Madzvamuse. A coupled bulk-surface model for cell polarisation. *J. Theor. Biol.*, 481:119–135, 2019.
- [5] A. Dhooge, W. Govaerts, and Y. A. Kuznetsov. MATCONT: a matlab package for numerical bifurcation analysis of odes. *ACM Trans. Math. Software (TOMS)*, 29(2):141–164, 2003.
- [6] L. Diambra, V. R. Senthivel, D. B. Menendez, and M. Isalan. Cooperativity to increase Turing pattern space for synthetic biology. *AVS Synthetic Biology*, 4:177–186, 2015.
- [7] X. Diego, L. Marcon, P. Müller, and J. Sharpe. Key features of Turing systems are determined purely by network topology. *Phys. Rev. X*, 8:021071, 2018.
- [8] E. Dulos, J. Boissonade, J. J. Perraud, B. Rudovics, and P. De Kepper. Chemical morphogenesis: Turing patterns in an experimental chemical system. *Acta Biotheor.*, 44:249, 1996.
- [9] C. M. Elliott, T. Ranner, and C. Venkataraman. Coupled bulk-surface free boundary problems arising from a mathematical model of receptor-ligand dynamics. *SIAM J. Math. Anal.*, 49(1):360–397, 2017.
- [10] R. Erban and J. Chapman. *Stochastic modeling of reaction-diffusion processes*. Cambridge Texts in Applied Mathematics, Cambridge U. Press, 2020.
- [11] A. Gierer. Generation of biological patterns and form: some physical, mathematical, and logical aspects. *Progress in biophysics and molecular biology*, 37:1–47, 1981.
- [12] A. Gierer and H. Meinhardt. A theory of biological pattern formation. *Kybernetik*, 12(1):30–39, 1972.
- [13] D. Gomez, S. Iyaniwura, F. Paquin-Lefebvre, and M. J. Ward. Pattern forming systems coupling linear bulk diffusion to dynamically active membranes or cells. *Phil. Trans. Roy. Soc. A.*, 379:20200276, 2021.
- [14] A. Gomez-Marin, J. Garcia-Ojalvo, and J. M. Sancho. Self-sustained spatiotemporal oscillations induced by membrane-bulk coupling. *Phys. Rev. Lett.*, 98:168303, 2007.
- [15] J. Gou, W.-Y. Chiang, P.-Y. Lai, M. J. Ward, and Y. X. Li. A theory of synchrony by coupling through a diffusive chemical signal. *Physica D*, 339:1–17, 2017.
- [16] J. Gou, Y. X. Li, W. Nagata, and M. J. Ward. Synchronized oscillatory dynamics for a 1-D model of membrane kinetics coupled by linear bulk diffusion. *SIAM J. Appl. Dyn. Sys.*, 14(4):2096–2137, 2015.
- [17] J. Gou and M. J. Ward. An asymptotic analysis of a 2-d model of dynamically active compartments coupled by bulk diffusion. *J. Nonlin. Sci.*, 26(4):979–1029, 2016.
- [18] J. Gou and M. J. Ward. Oscillatory dynamics for a coupled membrane-bulk diffusion model with Fitzhugh-Nagumo kinetics. *SIAM J. Appl. Math.*, 76(2):776–804, 2016.

- [19] P. Haas and R. Goldstein. Turing’s diffusive threshold in random reaction-diffusion systems. *Phys. Rev. Lett.*, 126:238101, 2021.
- [20] J. Halatek, F. Brauns, and E. Frey. Self-organization principles of intracellular pattern formation. *Phil. Trans. R. Soc. B*, 373(1747):20170107, 2018.
- [21] J Halatek and E Frey. Rethinking pattern formation in reaction–diffusion systems. *Nature Physics*, 14(5):507, 2018.
- [22] S. Iyaniwura and M. J. Ward. Synchrony and oscillatory dynamics for a 2-D PDE-ODE model of diffusion-mediated communication between small signalling compartments. *SIAM J. Appl. Dyn. Sys.*, 20(1):438–499, 2021.
- [23] V. Klika. Significance of non-normality-induced patterns: Transient growth versus asymptotic stability. *Chaos*, Jul;27(7):073120, 2017.
- [24] V. Klika, R. E. Baker, D. Headon, and E. A. Gaffney. The influence of receptor-mediated interactions on reaction-diffusion mechanisms of cellular self-organization. *Bull. Math. Bio.*, 74:935–957, 2012.
- [25] T. Kolokolnikov, M. J. Ward, and J. Wei. The stability of steady-state hot-spot patterns for a reaction-diffusion model of urban crime. *DCDS-B*, 19(6):1373–1410, 2014.
- [26] K. Korvasová, Gaffney E. A., Maini P. K., Ferreira M. A., and V. Klika. Investigating the Turing conditions for diffusion-driven instability in the presence of a binding immobile substrate. *J. Theor. Biol.*, 367:286–295, 2015.
- [27] A. Krause, E. A. Gafney, P. Maini, and V. Klika. Modern perspectives on near-equilibrium analysis of Turing systems. *Phil. Trans. R. Soc. A.*, 379:20200268, 2021.
- [28] A. Landge, B. M. Jordan, X. Diego, and P. Müller. Pattern formation mechanisms of self-organizing reaction-diffusion systems. *Dev Biol.*, 460(1):2–11, 2020.
- [29] I. Lengyel and I. R. Epstein. Modeling of Turing structures in the chlorite-iodide-malonic acid-starch reaction system. *Science*, 251:650, 1991.
- [30] H. Levine and W. J. Rappel. Membrane-bound Turing patterns. *Phys. Rev. E*, 72:061912, 2005.
- [31] A. Madzvamuse and A. H. W. Chung. The bulk-surface finite element method for reaction-diffusion systems on stationary volumes. *Finite Elem. Anal. Design*, 108:9–21, 2016.
- [32] A. Madzvamuse, A. H. W. Chung, and C. Venkataraman. Stability analysis and simulations of coupled bulk-surface reaction-diffusion systems. *Proc. R. Soc., Ser. A*, 471(2175):20140546, 2015.
- [33] P. Maini, K. Painter, and H. N. P. Chau. Spatial pattern formation in chemical and biological systems. *J. Chem. Soc. Faraday Trans.*, 93(1):3601–3610, 1997.
- [34] L. Marcon, X. Diego, J. Sharpe, and P. Müller. High throughput mathematical analysis identifies Turing networks for patterning with equal diffusing signals. *eLife*, 5:e14022, 2016.
- [35] P. Müller, K. W. Rogers, S. R. You, M. Brand, and A. F. Schier. Morphogen transport. *Development*, 140(8):1621–1639, 2013.
- [36] F. Paquin-Lefebvre, W. Nagata, and M. J. Ward. Pattern formation and oscillatory dynamics in a two-dimensional coupled bulk-surface reaction-diffusion system. *SIAM J. Appl. Dyn. Syst.*, 18(3):1334–1390, 2019.

- [37] F. Paquin-Lefebvre, W. Nagata, and M. J. Ward. Weakly nonlinear theory for oscillatory dynamics in a one-dimensional PDE-ODE model of membrane dynamics coupled by a bulk diffusion field. *SIAM J. Appl. Math.*, 80(3):1520–1545, 2020.
- [38] F. Paquin-Lefebvre, B. Xu, K. L. DiPietro, A. E. Lindsay, and A. Jilkin. Pattern formation in a coupled membrane-bulk reaction-diffusion model for intracellular polarization and oscillations. *J. Theor. Biol.*, 497:110242, 2020.
- [39] J. Pearson. Pattern formation in a (2+1)-species activator-inhibitor immobilizer system. *Physica A*, 188(1-3):178–189, 1992.
- [40] J. Pearson and W. Horsthemke. Turing instabilities with nearly equal diffusivities. *J. Chem. Phys.*, 90:1588, 1989.
- [41] A. Rätz and M. Röger. Turing instabilities in a mathematical model for signaling networks. *J. Math. Biol.*, 65(6-7):1215–1244, 2012.
- [42] A. Rätz and M. Röger. Symmetry breaking in a bulk–surface reaction–diffusion model for signalling networks. *Nonlinearity*, 27(8):1805, 2014.
- [43] Andreas Rätz. Turing-type instabilities in bulk–surface reaction–diffusion systems. *J. Comp. Appl. Math.*, 289:142–152, 2015.
- [44] E. M. Rauch and M. M. Millonas. The role of trans-membrane signal transduction in turing-type cellular pattern formation. *J. Theor. Biol.*, 226(4):401–407, 2004.
- [45] W. Ridgway, M. J. Ward, and B. T. Wetton. Quorum-sensing induced transitions between bistable steady-states for a cell-bulk ode-pde model with lux intracellular kinetics. *J. Math. Bio.*, 84(1-2), 2021.
- [46] L. M. Stolerman, M. Getz, S. Llewellyn Smith, M. Holst, and P. Rangamani. Stability analysis of a bulk-surface reaction model for membrane protein clustering. *Bull. Math. Bio.*, 82(2), 2020.
- [47] N. Tompkins, N. Li, C. Girabwe, and S. Fraden. Testing Turing’s theory of morphogenesis in chemical cells. *PNAS*, 111(12):4397–4402, 2014.
- [48] A. M. Turing. The chemical basis of morphogenesis. *Phil. Trans. Roy. Soc., Series B*, 237(641):37–72, 1952.
- [49] V. K. Vanag and I. R. Epstein. Localized patterns in reaction-diffusion systems. *Chaos*, 17(3):037110, 2007.
- [50] M. J. Ward. Spots, traps, and patches: Asymptotic analysis of localized solutions to some linear and nonlinear diffusive processes. *Nonlinearity*, 31(8):R189, 2018.
- [51] B. Xu and P. Bressloff. A PDE-DDE model for cell polarization in fission yeast. *SIAM J. Appl. Math.*, 76(3):1844–1870, 2016.
- [52] B. Xu and A. Jilkin. Modeling the dynamics of Cdc42 oscillation in fission yeast. *Biophysical J.*, 114(3):711–722, 2018.